Titre: Title:	Development of a New Biocompatible and Conductive Electrospun Patch for Cardiac Tissue Regeneration
Auteur: Author:	Clotilde Jugie
Date:	2024
Type:	Mémoire ou thèse / Dissertation or Thesis
Référence: Citation:	Jugie, C. (2024). Development of a New Biocompatible and Conductive Electrospun Patch for Cardiac Tissue Regeneration [Mémoire de maîtrise, Polytechnique Montréal]. PolyPublie. https://publications.polymtl.ca/59885/

URL de PolyPublie: PolyPublie URL:	https://publications.polymtl.ca/59885/
Directeurs de recherche: Advisors:	Abdellah Ajji, Michael R. Wertheimer, & Houman Savoji
Programme: Program:	Génie biomédical

POLYTECHNIQUE MONTRÉAL

affiliée à l'Université de Montréal

Development of a new biocompatible and conductive electrospun patch for cardiac tissue regeneration

CLOTILDE JUGIE

Institut de génie biomédical

Mémoire présenté en vue de l'obtention du diplôme de *Maîtrise ès sciences appliquées*

Génie biomédical

Septembre 2024

POLYTECHNIQUE MONTRÉAL

affiliée à l'Université de Montréal

Ce mémoire intitulé :

Development of a new biocompatible and conductive electrospun patch for cardiac tissue regeneration

présenté par **Clotilde JUGIE**

en vue de l'obtention du diplôme de *Maîtrise ès sciences appliquées*

a été dûment accepté par le jury d'examen constitué de :

Géraldine MERLE, présidente
Abdellah AJJI, membre et directeur de recherche
Houman SAVOJI, membre et codirecteur de recherche
Michel WERTHEIMER, membre et codirecteur de recherche
Marc LAVERTU, membre

ACKNOWLEDGEMENTS

This thesis would not have been possible without the support, guidance, and encouragement of many individuals. I would like to take this opportunity to express my deepest appreciation to all those who have helped me throughout this journey.

First and foremost, I am deeply indebted to my three supervisors, Professor Ajji, Professor Savoji, and Professor Wertheimer, whose expertise, patience, and constructive feedback have been invaluable to my research. Their unwavering support and insightful suggestions have guided me through the complexities of this work, and I am grateful for the opportunity to learn from them.

I would also like to extend my heartfelt thanks to the students from the different labs who shared their knowledge, time, and enthusiasm with me, the Alis, Arman, Cat-Thy, Saeideh, Elham, Aida, Sheyda, Alireza, and many more. Working alongside such talented and dedicated individuals has been an enriching experience, and I am grateful for the collaborative spirit that has made this research possible.

Special thanks are due to the research associates who played a crucial role in this project, Claire, Matthieu, Wendell. Their guidance in teaching me how to use the various machines and their assistance with troubleshooting were essential to the progress of my research. Their patience and willingness to share their expertise greatly contributed to my ability to navigate the technical aspects of this work.

Sur une note plus personnelle, je tiens à exprimer ma plus profonde reconnaissance à ma famille et à mes amis. À ma famille, votre amour inconditionnel, votre encouragement et votre foi en mes capacités m’ont permis de surmonter les moments les plus difficiles, même avec un océan nous séparant. À mes amis, merci pour votre soutien constant, votre compréhension, et pour avoir toujours été là pour me remonter le moral quand j'en avais le plus besoin.

Finally, I am grateful to everyone who, in one way or another, has been part of this journey. Your contributions, whether large or small, have played a significant role in bringing this work to fruition.

Thank you all.

RÉSUMÉ

Les maladies cardiovasculaires (MCV) demeurent la principale cause de mortalité dans le monde, les maladies cardiaques ischémiques étant responsables à elles seules de 16 % des décès mondiaux en 2019. Les traitements traditionnels, y compris la transplantation cardiaque, sont limités par la rareté des organes disponibles et la nécessité d'une immunosuppression à vie, ce qui souligne l'urgence de développer des thérapies alternatives. Les patchs cardiaques représentent une solution prometteuse, offrant un moyen de restaurer la fonction cardiaque en fournissant un soutien structurel et en favorisant la régénération du tissu cardiaque. Ce mémoire examine le développement de patchs biocompatibles et conducteurs produits par électrofilage pour l'ingénierie tissulaire cardiaque, en mettant l'accent sur la reproduction des propriétés structurelles, mécaniques et électriques du myocarde natif. L'étude a impliqué la sélection du polyuréthane (PU) comme matériau de base en raison de ses propriétés mécaniques favorables et de sa biocompatibilité. L'oxyde de graphène réduit (rGO) a été incorporé dans les fibres de PU pour améliorer la conductivité électrique, essentielle à la fonctionnalité des tissus cardiaques. Les fibres ont été produites par électrofilage, une technique connue pour créer des échafaudages de nanofibres ressemblant de près à la matrice extracellulaire des tissus cardiaques. Pour améliorer encore l'adhésion cellulaire, un revêtement riche en azote obtenu par polymérisation plasma (LPPE:N) a été appliqué. Les patchs obtenus ont été caractérisés par diverses techniques, notamment la microscopie électronique à balayage, des tests de traction et des mesures de conductivité. Les tests *in vitro* avec des fibroblastes cardiaques et des cardiomyocytes ont démontré la non-cytotoxicité des patchs, bien que l'impact du rGO et du revêtement LPPE:N sur la viabilité et l'adhésion cellulaire nécessite des études plus approfondies. Les résultats suggèrent que, bien que les patchs développés montrent un potentiel, une optimisation supplémentaire est nécessaire pour améliorer leurs performances dans les applications de régénération tissulaire cardiaque. Cette recherche contribue aux efforts continus en ingénierie tissulaire cardiaque, visant à offrir des alternatives viables aux thérapies conventionnelles pour les patients souffrant de MCV.

ABSTRACT

Cardiovascular diseases (CVDs) remain the leading cause of mortality worldwide, with ischemic heart diseases alone responsible for 16% of global deaths in 2019. Traditional treatments, including heart transplantation, are limited by the scarcity of donor organs and the need for lifelong immunosuppression, highlighting the urgent need for alternative therapies. Cardiac patches represent a promising solution, offering a means to restore heart function by providing structural support and enhancing cardiac tissue regeneration. This thesis investigates the development of biocompatible and conductive electrospun patches for cardiac tissue engineering, focusing on mimicking the structural, mechanical, and electrical properties of the native myocardium. The study involved the selection of polyurethane (PU) as the base material due to its favorable mechanical properties and biocompatibility. Reduced graphene oxide (rGO) was incorporated into the PU fibers to enhance electrical conductivity, which is critical for cardiac tissue functionality. The fibers were produced using electrospinning, a technique known for creating nanofibrous scaffolds that closely resemble the extracellular matrix of cardiac tissue. To further improve cell adhesion, a nitrogen-rich plasma-polymerized coating (LPPE:N) was applied. The resulting patches were characterized through various techniques, including scanning electron microscopy, tensile testing, and conductivity measurements. *In vitro* testing with primary cardiac fibroblasts and cardiomyocytes demonstrated the non-cytotoxicity of the patches, although the impact of rGO and LPPE:N coating on cell viability and adhesion requires further investigation. The findings suggest that while the developed patches show potential, additional optimization is needed to enhance their performance for cardiac tissue regeneration applications. This research contributes to the ongoing efforts in cardiac tissue engineering, aiming to provide viable alternatives to conventional therapies for patients suffering from CVDs.

TABLE OF CONTENTS

LIST OF TABLES

LIST OF FIGURES

LIST OF SYMBOLS AND ABBREVIATIONS

AuNP	Gold nanoparticles
BSA	Bovine serum albumin
CAR	Chimeric antigen receptor
CMs	Cardiomyocytes
CNTs	Carbon nanotubes
cTnT	Cardiac troponin T
CVDs	Cardiovascular diseases
C_2H_4	Ethylene
DAPI	4′,6-diamidino-2-phenylindole
DMF	Dimethylformamide
DMSO	Dimethyl sulfoxide
DPBS	Dulbecco's phosphate-buffered saline
ECM	Extracellular matrix
FAP	Fibroblast activation protein
FBS	Fetal bovine serum
IHDs	Ischemic heart diseases
LPPE:N	Low-pressure plasma-polymerized nitrogen-rich coating
MTT	(3-(4,5-dimethylthiazol-2-yl)-2,5-diphenyltetrazoliumbromid)
N	Nitrogen
NH_3	Ammonia
PANI	Polyaniline
PBS	Phosphate-buffered saline

PCL	Polycaprolactone
PEDOT:PSS	Poly(3,4-ethylenedioxythiophene) polystyrene sulfonate
PEG	Polyethylene glycol
PGS	Poly (glycerol sebacate)
PLA	Polylactic acid
PLGA	Poly(lactide-co-glycolide)
PPy	Polypyrrole
PS	Penicillin-streptomycin
PU	Polyurethane
PVA	Polyvinyl alcohol
RF	Radio frequency
rGO	Reduced graphene oxide
ROS	Reactive oxygen species
SEM	Scanning electron microscopy
TCP	Tissue culture plate
TFBA	4-trifluoromethyl-benzaldehyde
THF	Tetrahydrofuran
XPS	X-ray photoelectron spectroscopy

LIST OF APPENDICES

CHAPTER 1 INTRODUCTION AND LITERATURE REVIEW

1.1 Cardiovascular diseases

Cardiovascular diseases (CVDs) are the leading cause of mortality worldwide, accounting for 32% of all global deaths, constituting a significant health burden [1]. In Canada alone, as of 2017-2018, approximately 2.6 million individuals are diagnosed with CVDs, according to the Public Health Agency of Canada [2]. CVDs include diseases affecting different parts of the heart or blood vessels, among which are ischemic heart diseases (IHDs), responsible for 16% of global deaths in 2019 [3].

Primarily triggered by atherosclerosis of the coronary artery, wherein plaque buildup restricts or blocks blood flow, IHDs often culminate in catastrophic events like myocardial infarction. With their limited regenerative capacity, the resultant loss of cardiomyocytes (CMs) initiates fibrotic processes, transforming healthy myocardial tissue into non-contractile scar tissue [4]. Consequently, cardiac dysfunction, arrhythmias, and, in severe cases, cardiac arrest ensue. Figure 1.1 illustrates the process of atherosclerosis.

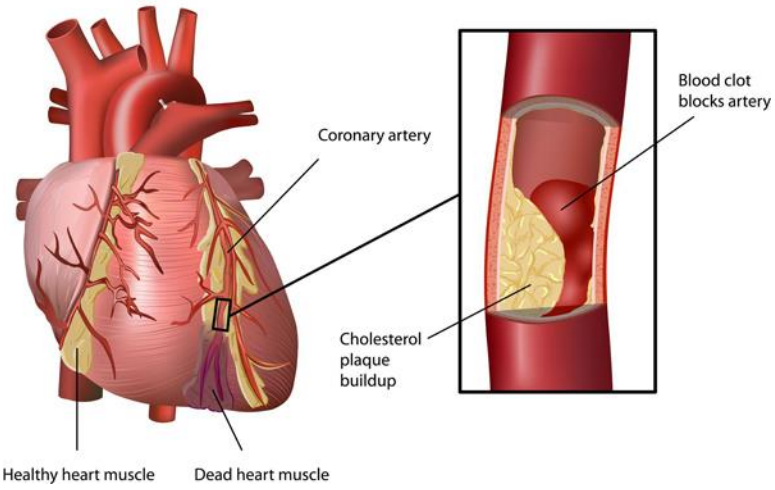

Figure 1.1 : Diagram of Atherosclerosis in the Coronary Artery. Reproduced from www.hri.org.au/health © 2024 HRI. All rights reserved.

While heart transplantation stands as a viable therapeutic recourse, its drawbacks, including the necessity for lifelong immunosuppressive medication to mitigate the risk of rejection, the scarcity

of suitable donor organs leading to prolonged waiting times and potential patient deterioration, as well as the inherent surgical risks such as infection and organ rejection [5], underline the urgency for the development of alternative treatments. Xenotransplantation, involving the use of genetically modified pig hearts, has been studied in non-human primates and, more recently, in two terminally ill patients [6]. Although both transplanted hearts initially functioned effectively, neither patient survived beyond two months post-procedure. This outcome was linked to several factors, with graft rejection being a key concern.

Cell therapy, an emerging approach involving the transplantation of healthy cells into damaged tissue, offers promise in cardiac regeneration. However, it grapples with significant challenges such as low cell engraftment rates, inconsistent clinical outcomes due to variations in cell types and delivery methods, and the imperative to ensure robust integration of transplanted cells with the host myocardium for sustained functional improvement [4], [7], [8]. While stem cells are commonly used in cell therapy, an alternative approach involves using a patient's own T cells. These T cells are genetically engineered to express a chimeric antigen receptor (CAR), enabling them to recognize specific proteins [9]. In the context of cardiac diseases, research has focused on targeting the fibroblast activation protein (FAP), which is expressed on the surface of activated fibroblasts (myofibroblasts). Cardiac fibroblasts differentiate into myofibroblasts during fibrotic processes, where they overproduce extracellular matrix (ECM) components, leading to scar tissue formation and tissue stiffening. By specifically targeting and depleting these pathological cells, CAR-T cells have the potential to reduce cardiac fibrosis, as illustrated in Figure 1.2 [10].

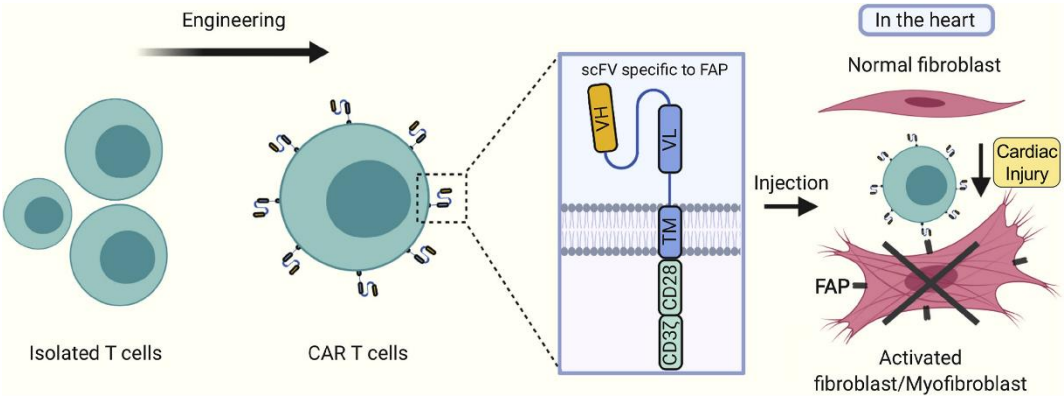

Figure 1.2 : CAR T Cells Engineering for Cardiac Injury Treatment. Reproduced from [10] © 2019 The Authors. All rights reserved.

However, several challenges remain, including ensuring T cell survival for an appropriate duration to avoid interfering with normal wound healing, managing immune-related side effects, and addressing the risk of macrophage infiltration, which may exacerbate fibrosis [9].

To reinforce the efficacy of cell therapy, researchers are exploring the integration of support structures—cardiac patches—that mimic the native ECM to facilitate tissue regeneration. Hence, it is imperative for cardiac patches to emulate the properties of the myocardium to enhance their therapeutic potential.

1.2 Cardiac tissue

Native cardiac tissue is primarily composed of CMs, blood vessels, and ECM, forming a highly organized structure essential for its function. The myocardium, which is the heart muscle, is responsible for the contractions and relaxations that pump blood throughout the body. CMs, the primary cell type in the heart, have a striated appearance due to organized sarcomeres. These cells are connected end-to-end by intercalated discs, which facilitate synchronized contraction through gap junctions and desmosomes [11]. These cells are represented in Figure 1.3, along with the anatomy of the heart [12].

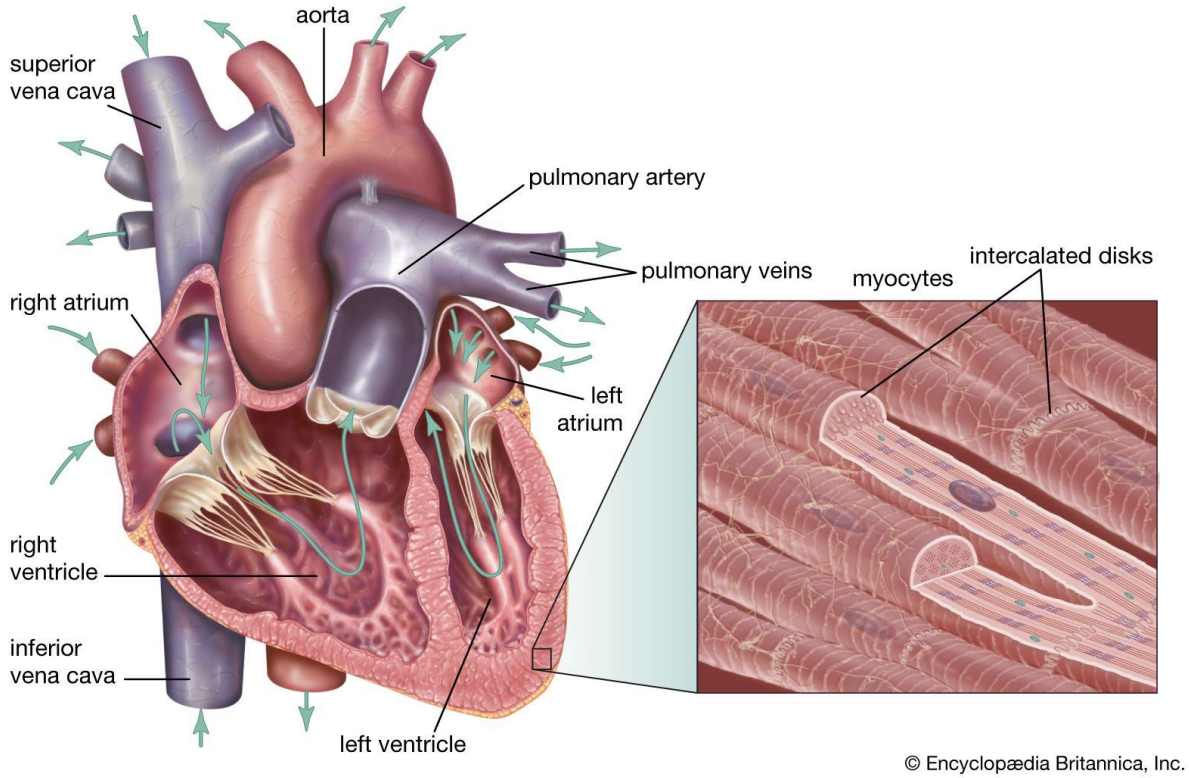

Figure 1.3 : Cross-section of a heart. Reproduced from [12] © 2024 Britannica, The Editors of Encyclopaedia. All rights reserved.

The ECM in cardiac tissue provides structural support and biochemical signals to the cells. It is composed of proteins like collagen, elastin, and glycoproteins, contributing to the tissue's elasticity and strength [13]. Additionally, a dense network of capillaries supplies oxygen and nutrients to the

CMs while removing metabolic waste, which is crucial for sustaining the high metabolic demand of the heart [7]. Figure 1.4 illustrates the composition of the cardiac ECM [14].

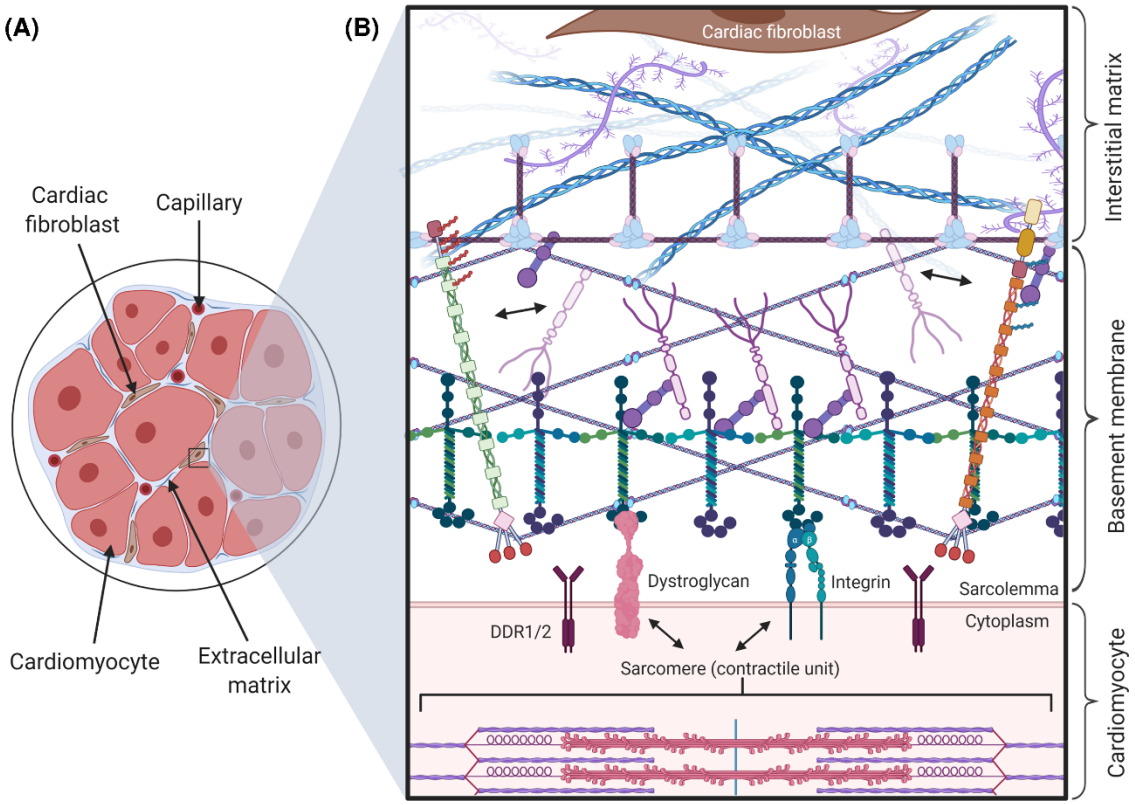

Figure 1.4 : Diagram of the cardiac ECM (basement membrane and interstitial matrix), including capillaries, fibroblasts, and cardiomyocytes. Several ECM molecules are represented (collagens, laminin, proteoglycans and glycoproteins). Reproduced from [14] © 2021 The Authors. All rights reserved.

Functionally, cardiac tissue's primary role is to contract rhythmically and forcefully, enabling the heart to pump blood. This is achieved through the coordinated contraction of CMs, driven by electrical impulses. Specialized cardiac cells, such as pacemaker cells in the sinoatrial node and the atrioventricular node, generate and propagate these electrical signals, regulating the heart's rhythm and ensuring the timely contraction of atria and ventricles [15].

The interplay of these structural components and their specific functions ensures the heart operates efficiently, maintaining circulation and delivering oxygen and nutrients to the body's tissues. Any disruption in the structure or function of cardiac tissue can lead to significant CVDs, emphasizing the importance of understanding and replicating these properties in cardiac tissue engineering.

1.3 Cardiac tissue engineering

Cardiac tissue engineering is a multidisciplinary field focused on creating biological substitutes that restore, maintain, or improve heart function [4], [7]. This approach aims to repair or replace damaged cardiac tissues (myocardium, cardiac valves, blood vessels…), enhancing the heart's ability to pump blood effectively. Figure 1.5 illustrates a bio-inspired design approach in the fabrication of nanofibrous scaffolds for cardiac tissue engineering.

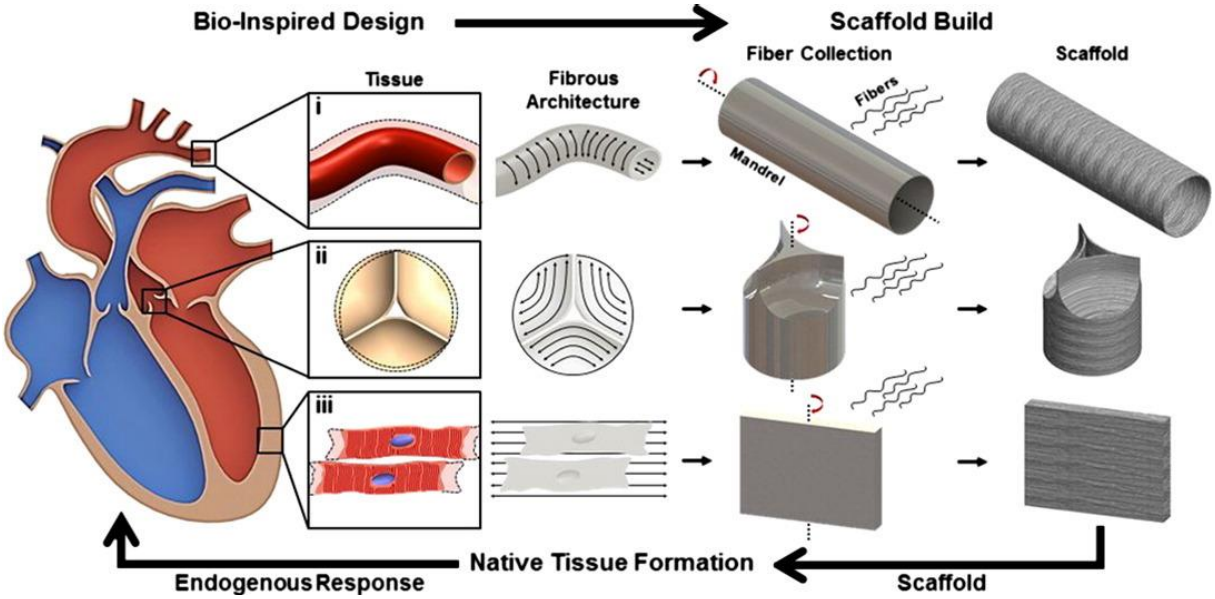

Figure 1.5 : Nanofibrous scaffolds for cardiac tissue engineering. Reprinted from A. K. Capulli, L. A. MacQueen, S. P. Sheehy, and K. K. Parker, "Fibrous scaffolds for building hearts and heart parts," Advanced Drug Delivery Reviews, vol. 96, pp. 83–102, Copyright (2016), with permission from Elsevier [11]

Strategies used in cardiac tissue engineering are either cell-based (stem cell therapy, cell sheet engineering) or scaffold-based, providing cells with a framework for regeneration, using fabrication techniques like 3D bioprinting [16], [17], hydrogels [18], [19], [20], or electrospinning [8], [11].

3D bioprinting excels in its precision, allowing for the controlled deposition of cells, biomaterials, and bioactive compounds to recreate the complex architecture of cardiac tissue, including essential vascular networks [16]. This technique enables the creation of customized heart structures that

closely resemble native tissues, using either extrusion, inkjet, or laser printing [17]. Challenges such as long-term cell survival, mechanical stability, and functional integration into the heart remain areas of ongoing research [16].

Hydrogels, on the other hand, provide a highly versatile, biocompatible scaffold that mimics the ECM, promoting cell survival, proliferation, and differentiation [19]. Their tunable mechanical properties allow them to replicate the heart's natural environment, while also enabling the controlled release of growth factors or signaling molecules to enhance tissue repair [18], [20]. Challenges remain in optimizing their mechanical properties for long-term function and ensuring proper vascularization in larger cardiac constructs [21], [22].

Finally, electrospinning is a versatile and effective technique for cardiac tissue engineering, enabling the creation of nanofibrous scaffolds that closely mimic the ECM, promoting tissue regeneration in cardiac repair applications. The principles and parameters of electrospinning will be discussed in detail in Section 1.5.

1.4 General criteria for cardiac patch fabrication

Focusing on myocardium regeneration, several general criteria for cardiac patch fabrication can be delineated. A cardiac patch must indeed possess specific mechanical, structural, electrical, and biological properties to be effective.

Mechanically, the cardiac patch should match the elasticity and strength of native cardiac tissue to endure the heart's dynamic environment [8], [11], [15], [23]. The native myocardium's Young's modulus, indicating stiffness, ranges from 10 to 20 kPa at the end of systole (contraction phase of the cardiac cycle) and from 200 to 500 kPa at the end of diastole (relaxation phase of the cardiac cycle) [24]. The tensile strength of the native myocardium ranges between 3 and 15 kPa [24]. During the cardiac cycle, the myocardium undergoes mechanical strain between 20 and 30% [11].

Structurally, a cardiac patch should closely replicate the native ECM by incorporating fibers with diameters typically ranging from 50 to 500 nanometers, reflecting the dimensions of collagen fibers found in the natural ECM [25]. Additionally, the patch should feature a highly porous network, essential for effective nutrient and oxygen diffusion, as well as for supporting cell infiltration and tissue integration [8], [23]. The alignment of fibers should correspond to the direction of applied stress, ensuring that the patch can adequately support the mechanical and functional demands of the heart. Such structural fidelity is crucial for achieving optimal tissue integration and function.

Electrically, the patch must conduct electrical impulses to synchronize with the heart's natural contractions, ensuring coordinated and effective pumping [8], [11], [15]. Native myocardium's effective extracellular longitudinal and transverse conductivities are considered to be 2.1 mS/cm and 0.5 mS/cm, respectively [26].

Biologically, the patch should promote cell adhesion, proliferation, and differentiation while being biocompatible and non-immunogenic to avoid adverse reactions [8], [15], [23]. It should, therefore, include binding sites for cells to support cell attachment and integration. Bioactive coatings for this purpose will be reviewed in section 1.7. Meeting the mechanical, structural, and electrical requirements will also inherently contribute to cell proliferation and differentiation.

By addressing these criteria, the development of an electrospun cardiac patch can advance toward effectively supporting myocardium regeneration and restoring heart function.

1.5 Electrospinning

Electrospinning is a versatile technique used to produce nanofibers from a wide array of materials, leveraging electrostatic forces to create fine, continuous fibers and offering numerous advantages that make it an excellent choice for the fabrication of cardiac patches. The electrospinning process is easy to execute, which facilitates potential up-scaling for broader clinical use [8]. One of the primary benefits of electrospinning is its ability to create structures with morphological similarities to the ECM. The resulting electrospun fibers can range from nano to micro scales, closely mimicking the ECM's continuous fibrous architecture. Additionally, electrospun constructs boast a high surface-to-volume ratio and high porosity. Another significant advantage of electrospinning is the ability to manipulate various parameters of the process to tailor the properties of the resulting fibers, enabling the optimization of the scaffold for specific cardiac applications.

Electrospinning, therefore, stands out as a superior option for fabricating cardiac patches due to its versatility, ease of processing, and ability to create ECM-like structures. Its potential for up-scaling and the customizable nature of the electrospun constructs make it a promising technology for advancing cardiac tissue engineering and improving patient outcomes.

1.5.1 Principle

The basic electrospinning process involves dissolving a polymer in a suitable solvent to form a viscous solution, which is then loaded into a syringe with a small-diameter needle [8]. An electric field is applied between the needle and a grounded collector, creating a high voltage that charges the polymer solution. As the electric field strength increases, it overcomes the surface tension of the solution, forming a Taylor cone at the needle tip [27]. When the electrostatic force exceeds the surface tension, a thin jet of the polymer solution is ejected.

The ejected jet undergoes stretching and thinning due to electrostatic repulsion and solvent evaporation, resulting in the formation of solid nanofibers. These fibers are collected on the grounded surface, creating a non-woven mat with a high surface area-to-volume ratio. Figure 1.6 presents a basic electrospinning setup [28].

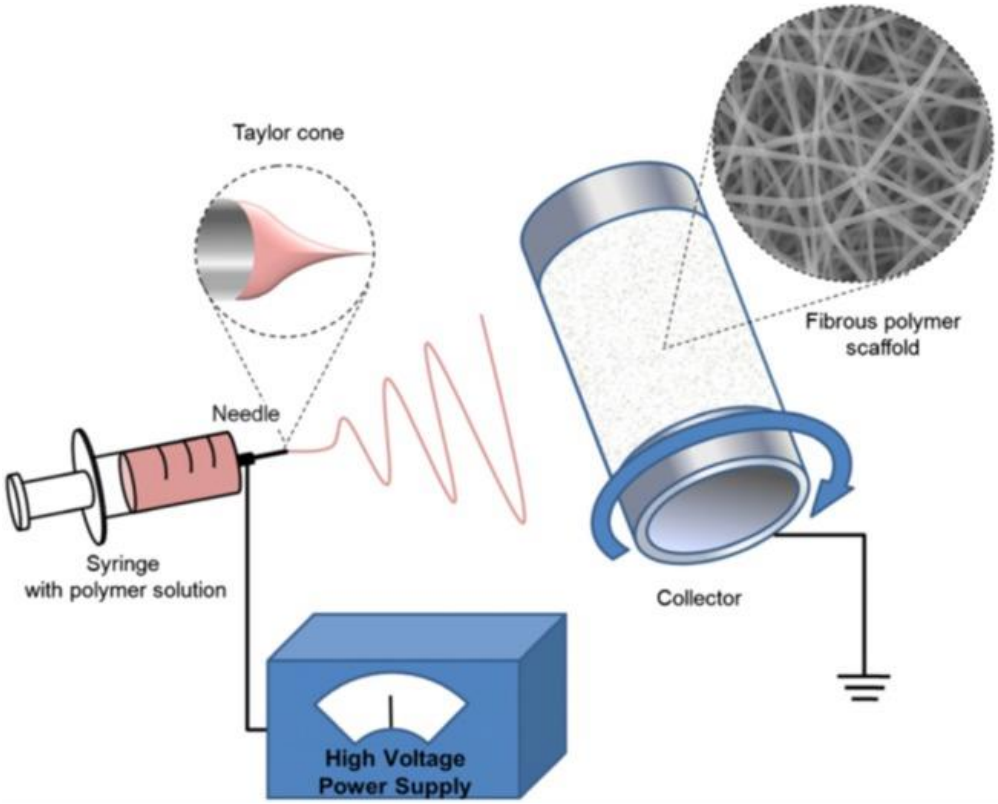

Figure 1.6 : Scheme of the electrospinning setup [28]. © IOP Publishing. Reproduced with permission. All rights reserved. N. G. Rim, C. S. Shin, and H. Shin, "Current approaches to electrospun nanofibers for tissue engineering," Biomed. Mater., vol. 8, no. 1, p. 014102, Jan. 2013, doi: 10.1088/1748-6041/8/1/014102

1.5.2 Parameters

In electrospinning, several key parameters influence the characteristics of the resulting fibers, which are critical for applications like cardiac tissue engineering. These parameters include process

conditions (voltage, flow rate, distance between needle and collector), the polymer solution properties, and ambient conditions [29].

- **Voltage:** The applied voltage creates the electrostatic forces necessary to form the polymer jet. Higher voltages generally produce thinner fibers but can lead to bead formation if too high, which is undesirable for uniform fiber mats.
- **Flow Rate:** The rate at which the polymer solution is fed through the needle affects fiber diameter and morphology. A higher flow rate increases fiber diameter but may result in uneven fiber deposition and beads due to insufficient solvent evaporation.
- **Distance:** The distance between the needle and collector determines the flight time of the polymer jet, impacting fiber formation and solvent evaporation. An optimal distance ensures complete solvent evaporation and uniform fiber deposition without bead formation.
- **Solution Properties:** Viscosity, conductivity, and surface tension of the polymer solution also play significant roles. Proper solvent selection and polymer concentration are crucial for stable jet formation and smooth fiber production.
- **Ambient Conditions:** Temperature and humidity affect solvent evaporation and fiber morphology. Controlled environmental conditions ensure consistent fiber quality.

For cardiac tissue engineering, the goal is to produce fibers that mimic the ECM, promoting cell attachment, proliferation, and differentiation. This requires fine-tuning of parameters to achieve fibers with appropriate diameters, mechanical properties, and surface morphology, described earlier. Achieving a balance between voltage, flow rate, distance, optimized solution properties, and controlled ambient conditions can result in electrospun fibers suitable for developing cardiac patches that effectively integrate with native tissue and support cardiac function.

1.6 Electrospinning materials for cardiac tissue engineering

By manipulating the electrospinning parameters, researchers can tailor the physical and chemical properties of the scaffolds to meet the specific requirements of cardiac tissue regeneration. Another important factor in meeting those requirements is the choice of electrospinning materials. The following sections will delve into the diverse materials utilized in electrospinning for cardiac applications, highlighting natural polymers, synthetic polymers, and the incorporation of conductive materials to enhance the functionality of the engineered cardiac tissues.

1.6.1 Natural polymers

Natural polymers are widely used in electrospinning for cardiac tissue engineering due to their biocompatibility and resemblance to the ECM. Common examples include collagen, gelatin, chitosan, and silk fibroin.

A major component of the ECM, collagen supports cell adhesion, proliferation, and differentiation. Electrospun collagen fibers provide a biomimetic scaffold that promotes tissue regeneration. The addition of collagen to polylactic acid/polyethylene glycol (PLA/PEG) nanofiber patches [30] led to a notable increase in cell viability, especially in the aligned patches, which showed a cell viability rate of 143% at day 3 of CMs culture compared to below 50% for PLA/PEG patches. Additionally, the aligned nanofiber patches with collagen supported more homogeneous and organized cell growth compared to random ones.

Derived from collagen, gelatin retains similar properties and is more soluble, making it easier to electrospin. In this study [31], CMs on polycaprolactone (PCL)/Gelatin electrospun scaffolds showed enhanced viability at a higher gelatin ratio (60% gelatin/40% PCL).

Obtained from chitin, chitosan has antibacterial properties and supports cell attachment and growth. It is often blended with other polymers to enhance its mechanical properties. In this study [32], chitosan-containing PLA electrospun scaffolds exhibited better CMs viability at a ratio of 7:1 PLA

to chitosan for aligned fibers, as well as higher levels of sarcomeric α-actinin and troponin I expression, indicating improved cell function and maturation.

Silk fibroin is known for its excellent mechanical strength and biocompatibility, it supports cell adhesion and growth, making it suitable for cardiac applications. Reduced graphene oxide/silk fibroin electrospun matrices [33] exhibited high cell viability and proliferation of CMs and myocardial fibroblasts, with both cell types showing >99% viability during a 7-day culture period. Additionally, the silk fibroin-based scaffolds improved post-myocardial infarction outcomes of infarcted rats.

Natural polymers offer several advantages in cardiac tissue engineering. Their inherent biocompatibility and biodegradability reduce the risk of adverse immune responses and facilitate integration with native tissue [15], [23]. They provide a supportive environment for cell attachment, proliferation, and differentiation, which is crucial for effective cardiac tissue regeneration. Additionally, their resemblance to the natural ECM enhances their ability to promote tissue healing and repair [15].

Despite their benefits, natural polymers also present challenges. They often have lower mechanical strength compared to synthetic polymers [15], [23], which can limit their application in load-bearing cardiac tissues. Their properties can vary based on their source and extraction method, leading to inconsistencies in scaffold performance [23]. They may also be more challenging to process compared to synthetic polymers, requiring careful optimization of electrospinning parameters to achieve desired fiber properties [15]. Moreover, natural polymers may degrade too quickly, mismatching the tissue regeneration timeline [15], [23].

1.6.2 Synthetic polymers

Synthetic polymers are widely used in electrospinning for cardiac tissue engineering due to their tunable properties and reproducibility. Examples include polyurethane (PU), polylactic acid (PLA) and copolymer poly(lactide-co-glycolide) (PLGA), polycaprolactone (PCL), and poly(glycerol sebacate) (PGS).

PU is known for its excellent mechanical properties, flexibility, and biocompatibility, which makes it suitable for creating durable cardiac patches that can withstand the dynamic environment of the heart. PU scaffolds exhibited good elasticity, while the addition of carbon nanotubes (CNTs) enhanced tensile strength and stiffness [34]. Moreover, PU/CNTs nanocomposites showed good cytocompatibility with CMs and human umbilical vein endothelial cells (HUVECs).

PLA and PLGA are biodegradable polymers favored for their ease of processing and controlled degradation rates, which can be tailored to match tissue regeneration timelines. Constructs made from PLGA/gelatin/polypyrrole nanoparticles supported cell attachment, proliferation, and viability, showing over 98% cell viability for various cell types, including CMs, over 14 days [35]. These scaffolds also demonstrated consistent degradation over 15 days.

PCL is appreciated for its slow degradation rate and superior mechanical properties, making it ideal for long-term applications. PCL scaffolds coated with ECM proteins, when electrospun into aligned microfibers, significantly enhance the organization and function of CMs derived from induced pluripotent stem cells [36]. Results show that the aligned PCL scaffolds promote greater CMs alignment, increased sarcomeric length, and upregulation of the MYH7 gene, which are indicators of improved cellular maturity and contractility compared to randomly oriented scaffolds.

PGS is a biodegradable elastomer known for its excellent biocompatibility and mechanical properties, which can be precisely tailored for specific applications. In this study [13], when blended with gelatin, PGS creates nanofibrous scaffolds that exhibit tunable mechanical properties and structural integrity, supporting cardiac fibroblasts and CMs attachment, proliferation, and alignment. The scaffolds demonstrate variable stiffness and elasticity, which can be precisely controlled by adjusting the PGS content.

The benefits of synthetic polymers include their superior mechanical strength [15], [23], which provides the necessary durability for cardiac applications. Their properties can be precisely controlled through polymer synthesis and blending, allowing customization according to specific tissue engineering needs [15], [23]. Synthetic polymers also offer consistent quality and properties [15], [23], ensuring reliable performance and easier scalability for clinical applications.

However, some synthetic polymers may elicit inflammatory responses or have limited biocompatibility, necessitating additional surface modifications or blending with natural polymers to enhance cell interactions [15]. Unlike natural polymers, synthetic polymers do not inherently

support cellular activities such as adhesion and proliferation, which can limit their effectiveness unless bioactive molecules or coatings are incorporated.

1.6.3 Conductive materials incorporation

Incorporating conductive materials into electrospinning constructs is crucial for cardiac tissue engineering due to the importance of electrical conductivity in cardiac patches, as previously stated in section 1.4. Examples of conductive materials used in electrospinning include carbon nanotubes, graphene, reduced graphene oxide, gold nanoparticles, polypyrrole, polyaniline, and poly(3,4-ethylenedioxythiophene) polystyrene sulfonate.

Carbon nanotubes (CNTs) are known for their excellent electrical conductivity and mechanical strength [37], [38]. When incorporated into electrospun fibers, CNTs can enhance the electrical properties of the scaffold, promoting better cell communication and function. However, CNTs can be challenging to disperse uniformly in polymer solutions, and their potential cytotoxicity necessitates careful consideration [38]. In this aforementioned study [34], incorporating CNTs to electrospun PU improved the electrical conductivity of the scaffolds, promoting better CM communication and function.

Graphene, a single layer of carbon atoms arranged in a hexagonal lattice, offers outstanding electrical conductivity and mechanical properties [37], [38]. Its incorporation into electrospun fibers can improve cardiac patches' electrical and structural integrity. Yet, graphene's hydrophobic nature and potential aggregation pose challenges for uniform dispersion and biocompatibility [37]. A study found that the addition of 1% wt graphene in PCL/PGS electrospun scaffolds resulted in the highest cell adhesion and CMs viability, compared to lower graphene percentage [39].

Reduced graphene oxide (rGO) retains many of graphene's conductive properties but with better dispersibility in aqueous solutions due to its functional groups [37], [38]. rGO can enhance the electrical conductivity of electrospun fibers while being more biocompatible than pristine graphene. In this study [40], rGO incorporated into poly(L-lactide-co-ε-caprolactone) (PLCL) electrospun fibers significantly enhanced the electrical conductivity of the scaffolds, promoting better CMs coupling, maturation, and synchronous electrical conductivity.

Gold nanoparticles (AuNPs) are another example of conductive materials used in electrospinning. They provide excellent conductivity and biocompatibility, promoting cell proliferation and differentiation [37], [38]. However, their high cost and potential for agglomeration can limit their practical application [37]. In this study [41], AuNPs were evaporated onto PCL-gelatin fibers, resulting in enhanced electrical conductivity, promoting the assembly of more elongated and aligned cardiac tissues, maintaining a higher ratio of CMs to fibroblasts, and increasing cardiac sarcomeric actinin expression. Furthermore, the engineered cardiac tissues within these AuNP scaffolds exhibited significantly higher contraction amplitudes and rates compared to those without gold, demonstrating improved functionality.

Polypyrrole (PPy) is a conductive polymer that offers good electrical conductivity and biocompatibility [37], [38]. Its incorporation into electrospun fibers can improve electrical signaling and mechanical properties, but its brittleness and potential for oxidative degradation are challenges that need to be addressed [37], [38]. In the previously referenced study [35], PPy was blended with other polymers to enhance CM electrochemical coupling, promoting better consistency and efficiency of cell contractions. However, the inclusion of PPy nanoparticles within electrospun fibers resulted in higher conductivity but also decreased the elongation percentage, indicating a trade-off between mechanical strength and electrical conductivity.

Polyaniline (PANI) is another conductive polymer known for its electrical conductivity and ease of synthesis [37], [38]. It can be incorporated into electrospun fibers to enhance electrical properties. However, PANI's biocompatibility and stability under physiological conditions require further optimization [37]. A study demonstrated that incorporating PANI into electrospun collagen/hyaluronic acid fibers enhances their electrical properties while maintaining biocompatibility and mechanical strength [42]. PANI-containing fibers showed improved electrical conductivity, supporting CM attachment and contractions. However, the study noted that higher concentrations of PANI led to increased cytotoxicity.

PEDOT:PSS (poly(3,4-ethylenedioxythiophene) polystyrene sulfonate) is a highly conductive polymer that combines the excellent conductivity of PEDOT with the water solubility and film-forming properties of PSS. PEDOT:PSS offers good biocompatibility and mechanical flexibility, making it an attractive choice for electrospun cardiac patches [37], [38]. However, its conductivity can be affected by processing conditions and it may require additional stabilization for long-term

applications [37], [38]. The incorporation of PEDOT:PSS into chitosan/polyvinyl alcohol (PVA) scaffolds significantly enhanced their electrical conductivity, mechanical properties, biocompatibility, and cell viability [43]. Specifically, the electrical conductivity of the scaffolds increased by approximately 100-fold, as did the tensile strength, with the addition of PEDOT:PSS.

1.7 Bioactive coatings – Focus on plasma polymerization

Bioactive coatings play a crucial role in cardiac tissue engineering by enhancing the interaction between engineered materials and native cardiac tissue. By incorporating bioactive molecules such as growth factors, peptides, or other signaling compounds, these coatings create a more favorable environment for cell growth and tissue healing, mimicking the natural ECM [15]. This is particularly important for synthetic polymers-based scaffolds due to their low biocompatibility, as stated in section 1.6.2.

Molecules applied to scaffolds include various ECM proteins such as collagen and fibronectin, polysaccharides like hyaluronic acid and chitosan, and growth factors [8]. Additionally, specific functional groups, such as RGD peptides, can be incorporated to mimic cell adhesion motifs found in natural ECM proteins. These molecules can be applied through methods such as adsorption, chemical surface functionalization, and layer-by-layer assembly [44].

Plasma polymerized coatings represent another cutting-edge approach to bioactive surface modification. The process involves the generation of a plasma, which is a partially ionized gas containing ions, electrons, and neutral species, by applying an electric field to a gas (Figure 1.7) [45]. This plasma state enables the activation and fragmentation of gas-phase monomers, which then polymerize and deposit onto a substrate as a thin, conformal coating. The resulting

polymerized film can be tailored to possess specific chemical functionalities and surface properties, making it particularly suitable for cardiac applications.

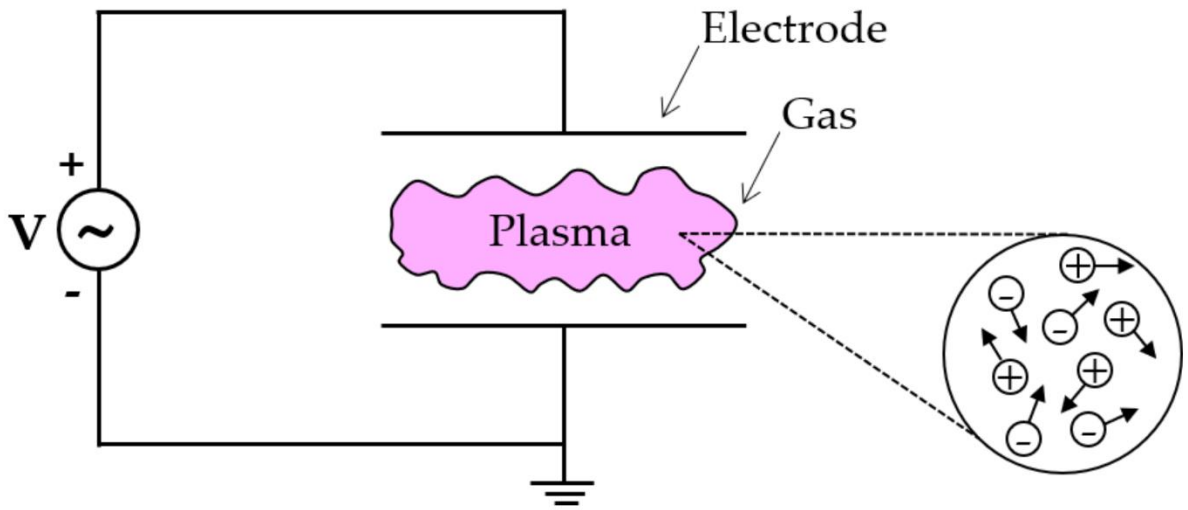

Figure 1.7 : Schematic view of a plasma generated between two electrodes. Reproduced from [45] © 2021 by the authors. License MDPI, Basel, Switzerland.

Amino ($-NH_2$), carboxyl (-COOH), hydroxyl (-OH), sulfhydryl (-SH), and aldehyde (-CHO) groups can be incorporated to plasma polymerized coatings to improve cell adhesion and promote specific cellular responses, through the use of different gases [46]. For example, one study demonstrated that an amine-rich plasma polymerized coating (LPPE:N) produced with a mixture of ethylene and ammonia gases significantly enhanced HUVECs adhesion and growth on electrospun poly(ethylene terephthalate) (PET) nanofiber mats [47]. The LPPE:N coating also improved HUVEC resistance to flow-induced shear stress, leading to a near-confluent endothelial cell monolayer on the topmost surface of the scaffold, which is advantageous for vascular graft applications.

The functional groups incorporated by plasma polymerization can also serve as reactive sites for further chemical modifications or the conjugation of bioactive molecules. For example, in one study [48], an oxygen-rich coating was deposited on PCL/eggshell scaffolds using plasma generated with ethylene gas and molecular oxygen diluted in argon gas. This plasma polymerization process introduced oxygen-containing functional groups to the surface, which were subsequently used to graft gentamicin. This modification resulted in significant antibacterial

activity against Pseudomonas aeruginosa, with bacterial reduction rates reaching 99.94% after 24 hours of incubation, as well as high biocompatibility with 90% cell viability.

Plasma polymerized coatings provide several advantages, including the introduction of high-density and stable functional groups, which are more effective than conventional plasma-induced grafting [47]. Additionally, the mild plasma conditions used ensure that the properties of polymeric mats remained unaffected. Earlier studies have already proven that the LPPE:N coating is highly effective, reproducible, and sufficiently stable over time for cell culture applications [49], [50], [51].

In summary, plasma-polymerized coatings provide a versatile and effective means of enhancing the surface properties of materials used in tissue engineering. By using different plasma gases, it is possible to introduce specific functional groups that tailor the surface for improved biocompatibility and performance, making them highly valuable for developing effective cardiac patches and advancing cardiac tissue engineering.

CHAPTER 2 OBJECTIVES AND PROPOSED APPROACH

The clinical translation of cardiac patches faces several challenges, including suboptimal cell engraftment, inadequate mechanical and electrical integration with native tissues, and immunological concerns [4], [7]. However, the reviewed techniques and materials present promising solutions that can be combined to enhance the properties of engineered cardiac patches, effectively addressing these challenges.

Hypothesis

The general hypothesis of this research project is that a cardiac patch fabricated using electrospinning of conductive biomaterials and plasma polymerization can be engineered to exhibit mechanical, electrical, and biological properties that closely mimic those of native myocardium, thereby improving cardiac tissue engineering outcomes.

General objective

The general objective of this research project is to develop and characterize electrospun cardiac patches that replicate the structural, mechanical, electrical, and biological properties of native myocardium for application in cardiac tissue engineering.

Specific objectives

The specific objectives of this research project are the following :

1. Identify and select an electrospinnable polymer with mechanical properties as close as possible to native cardiac tissue.
2. Fabricate and characterize the electrospun patch to ensure it meets the mechanical, electrical, and structural properties essential for cardiac tissue engineering.
3. Assess the *in vitro* biological properties of the developed patch, including biocompatibility and cell adhesion, using relevant cardiac cells.

Proposed approach

To achieve these objectives, the proposed approach includes using medical-grade PUs (Figure 2.1 A [52]) as electrospinning materials due to their proven biocompatibility, biostability, consistent quality, and their elastomeric properties, which are crucial for cardiac tissue engineering as described in Section 1.4. Additionally, rGO (Figure 2.1 B [53]) will be incorporated as a conductive element in the electrospun fibers because of its high conductivity, enhanced biocompatibility compared to other reviewed conductive materials, and availability due to synthesis in our laboratory. The production of electrospun mats will combine randomly oriented fibers with aligned fibers on top, achieving surface alignment beneficial for cardiomyocyte maturation, as highlighted in reviewed studies. This arrangement also ensures the moderation of mat's stiffness due to the lower elastic modulus of the randomly oriented fibers, forming the bulk of the construct. Furthermore, a nitrogen-rich plasma polymerized coating will be applied to enhance cell adhesion properties through a simple one-step process, which the grafting of an immunomodulatory molecule could accompany in a future study. Figure 2.1 C) summarizes the structure of the proposed approach.

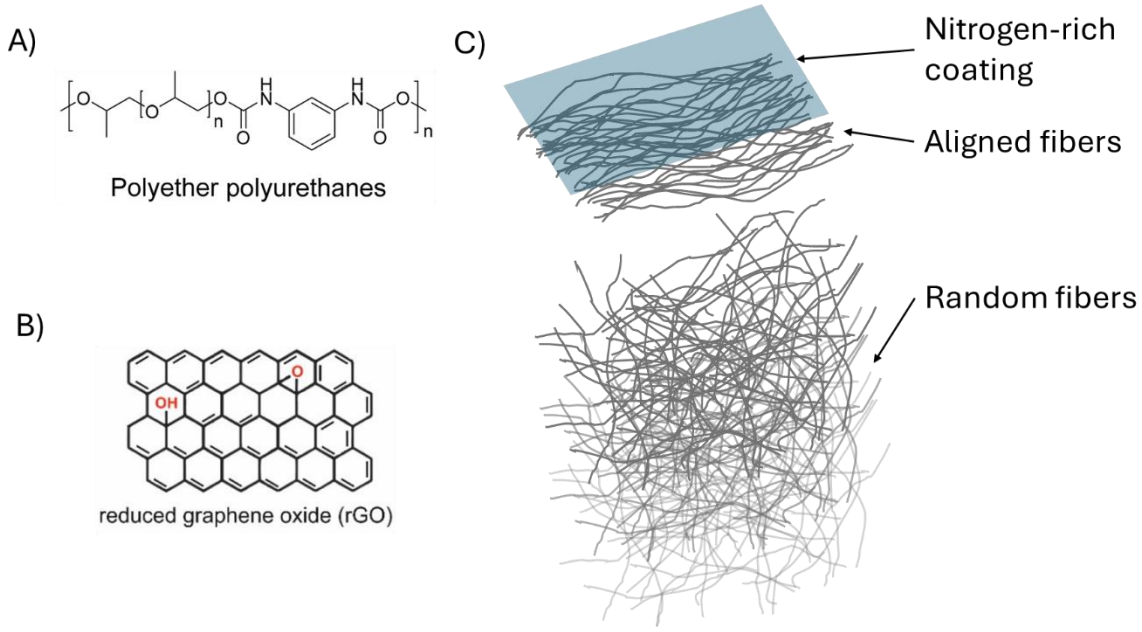

Figure 2.1 : A) Chemical structure of polyether PUs. Reproduced from [52] with permission. © 2021 Wiley Materials. All rights reserved. B) Chemical structure of rGO. Reproduced from [53]. © 2018 The Authors. All rights reserved. C) Diagram of the proposed patch's structure.

CHAPTER 3 METHODS

3.1 Material selection

To develop a patch that closely mimics the mechanical properties of native myocardium, several of the previously mentioned polymers were evaluated before ultimately selecting PU. Initial electrospinning trials using two medical-grade PUs from Lubrizol Advanced Materials were performed, followed by tensile testing of the produced mats, to refine the choice and optimize material selection.

3.1.1 Preliminary electrospinning

Electrospinning solutions preparation

7wt% Tecoflex™ SG-80A PU or 5wt% Tecophilic™ SP-80A-150 PU pellets were dissolved in Tetrahydrofuran (THF) and Dimethylformamide (DMF) (1:1), and the solution was stirred magnetically overnight before electrospinning.

Electrospinning parameters

The electrospinning solutions were loaded in a plastic syringe and electrospun through a 21G needle in a homemade horizontal electrospinning set-up. The distance between the needle tip and the mandrel collector was 15 cm, the voltage was 15 kV, and the flow rate was 1.5 mL/h. The fibers were collected on an aluminum foil placed around the mandrel, rotating at 175 rpm (diameter 10 cm). After electrospinning, the mats were allowed to dry in ambient air.

3.1.2 Preliminary tensile tests

The preliminary tensile tests were performed on the uniaxial tensile testing machine ElectroPuls E3000 from Instron equipped with a 250 N load cell at a speed of 5 mm/min. The initial gauge

length between the pneumatic grips was 10 mm, and the samples' width was about 20 mm. To facilitate the manipulation of the samples, they were mounted between the grips with the aluminum foil, which was peeled off and cut only in the middle.

3.2 Mats fabrication

3.2.1 Electrospinning

Electrospinning solutions preparation

Without rGO

Tecophilic™ SP-80A-150 PU pellets were dissolved in a 2:1 mixture of THF and DMF at a concentration of 5wt%. The solution was stirred magnetically overnight before electrospinning.

With rGO

rGO was ultrasonicated in DMF for 1h before the addition of THF and Tecophilic™ SP-80A-150 PU pellets to obtain a final solution of 5wt% PU, 0.5% or 1% rGO, with a 2:1 ratio of THF and DMF. The solution was then stirred overnight and bath sonicated for 5 min just before electrospinning.

Electrospinning parameters

The electrospinning solution was loaded into a syringe to which a 21G needle was attached. The syringe was placed in the Tong Li top-down electrospinning setup. The flow rate was set at 1.5 mL/h, and the mandrel (10 cm diameter) rotation speed at 50 rpm to make randomly oriented fibers (hereafter referred to as random fibers) or 1000 rpm to make aligned fibers. To make a mat with random fibers and aligned fibers on top, $5/6^{th}$ of the solution was electrospun with a rotation speed of 50 rpm, then the rest at 1000 rpm. The needle translated along the length of the mandrel at a speed of 10 mm/s. For a solution without rGO, the voltage was set at 14 kV and the distance between the needle tip and the collector at 14 cm, while for a solution with rGO, they were set respectively at 15 kV and 15 cm.

After electrospinning, mats were carefully peeled off the aluminum foil and allowed to dry in ambient air before the mats were used.

3.2.2 Plasma polymerized coating

To enhance cell adhesion on the mats, a previously developed coating (LPPE:N) was applied on them [54]. Electrospun samples were fixed in a low-pressure chamber where a plasma was formed and maintained through feeding ethylene (C_2H_4) and ammonia (NH_3) gases and an applied RF current. The pressure was around 600 mTorr, and the flow rates of ethylene and ammonia gases were 20 and 15 sccm, respectively. The power was set at 15 W, and the samples were exposed to the plasma for 15 minutes. Figure 3.1 represents the reactor used for this process. Coated samples were used a maximum of four days after coating.

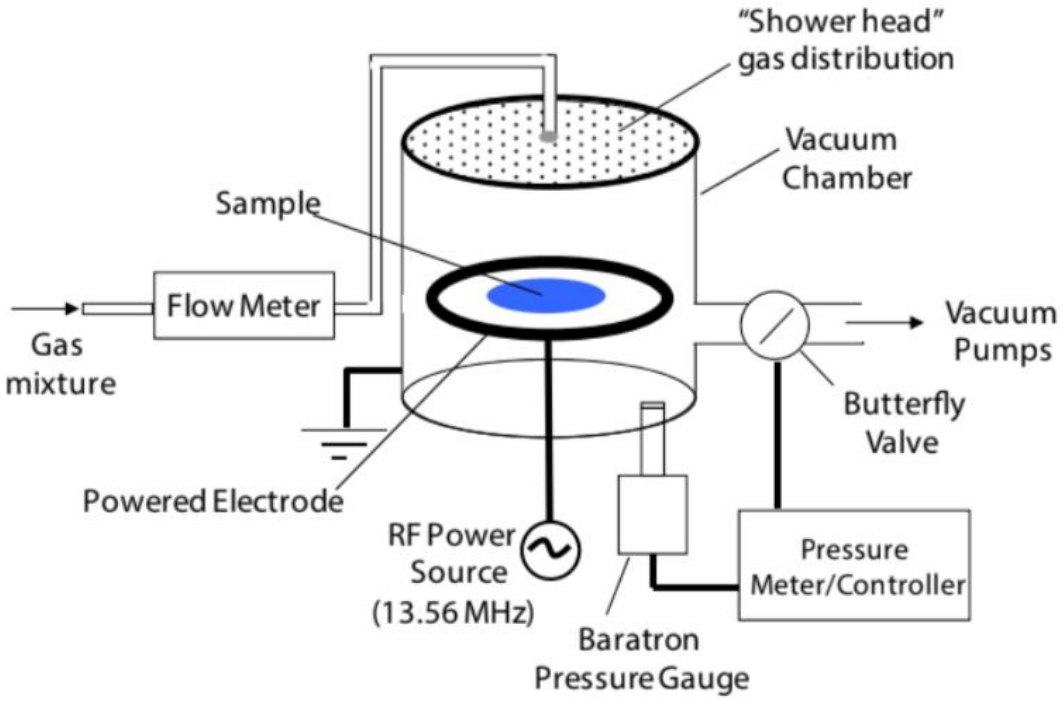

Figure 3.1 : Schematic views of the low-pressure capacitively-coupled r.f. reactor, used for depositing nitrogen-rich thin organic coating. Reproduced with permission from [54]. Copyright © 2008 WILEY-VCH Verlag GmbH & Co. KGaA, Weinheim

3.3 Mats characterization

3.3.1 Scanning electron microscopy

Electrospun mat surfaces were sputter-coated under vacuum with a thin layer of chromium (20 nm) and were then fixed with double-sided tape on a sample holder to image them with scanning electron microscopy (SEM) at 15 kV.

ImageJ software (NIH) was used to determine the diameter of the fibers of electrospun mats. 5 different images were used for each mat, and diameter measurement was performed for 20 fibers per image, for a total of 100 fibers for each mat.

Similarly, the orientation of fibers – expressed as degrees (0 to 180) – was determined for 100 fibers across 5 images for each mat. A line was traced along the orientation of each fiber and its angle was recorded, horizontal and vertical lines having 0° and 90° angles, respectively.

3.3.2 Surface chemical analysis (XPS)

X-ray photoelectron spectroscopy (XPS) analyses were performed in Polytechnique's LASM laboratory using a VG ESCALAB 250Xi, with a monochromatic Al Ka source operated at 14.7 kV, 14.9 mA. The size of the analyzed area was about 1 mm^2, and the sampling depth was under 10 nm. Spectra were acquired at 0° emission angles (normal to the mat surface). Quantification of data was performed using Avantage v4.12 software (Thermo Fisher Scientific) using integral peak intensities and sensitivity factors from the Al Thermo table, and charging was corrected by referencing all peaks to the carbon (C1s) peak at binding energy 285.0 eV.

3.3.3 Tensile tests

Tensile testing of the electrospun mats was performed with Biomomentum's Mach-1, using a 10 N load cell and 20 mm/min testing speed. The width of the samples was about 10 mm, while the

gauge length between the two grips was 23 mm. Mats' thickness was measured with a micrometer at 3 different points and averaged. 5 samples were tested for each mat.

For the testing of wet mats, they were submerged in deionized water 24h prior to testing.

The force and position were recorded until the break of the sample or axis course limit was reached (~10 cm). Load, tensile stress, and tensile strain were calculated from this data and the sample's dimensions, then the stress-strain curve was traced. Young's modulus and tensile strength were determined from the curves.

3.3.4 Conductivity tests

Volume resistivity measurements were performed using Keithley 6517A resistivity meter coupled with resistivity test fixture 8009, samples' dimensions being larger than 54 mm. Fibers were randomly oriented, and the mean thicknesses of PU, PU rGO0.5%, PU rGO1% mats were respectively 400, 660, 1050 µm. 1 volt was applied at the top electrode, and the current measured by the bottom electrode was recorded. The value after 60 seconds of electrification was retained, and conductivity was calculated using the following formulas:

$$\sigma_v = \frac{1}{\rho_v}\ S/cm\ , \qquad \rho_v = \frac{22.9V}{tI}\ \Omega.cm \tag{3.1}$$

where: σ_v is the volume conductivity.

ρ_v is the volume resistivity.

22.9 is the surface area of the sample under the test electrode.

V is the applied test voltage.

t is the average thickness of the sample.

I is the current reading.

The values for 3 replicates per mat were recorded.

3.4 *In vitro* testing

3.4.1 Samples preparation

The produced electrospun mats were cut into disks of different diameters to fit into wells of different sizes, depending on the experiment conducted. They were then sterilized by wetting and washing them in an antibiotic solution (1% Penicillin/Streptomycin (PS) in PBS), and subsequently placed under UV light for at least 90 minutes.

3.4.2 Cell culture

Primary cardiac fibroblasts were previously harvested in the lab from neonatal Sprague-Dawley rats and frozen following standard protocols. To be used in the following experiments, they were thawed and plated in a culture flask for amplification in a cell medium consisting of DMEM/F12 supplemented with 10% Fetal Bovine Serum (FBS) and 1% PS. They were placed in a humidified incubator at 37°C and 5% CO_2 atmosphere, and the cell medium was changed every 2 or 3 days until a confluence of around 80% was reached. The cells were then detached by trypsinization and counted to be seeded for further experiments. They were used between passages 3 and 6.

3.4.3 Indirect cytotoxicity assessment

To assess the indirect cytotoxicity of the electrospun mats, cells were cultured in a medium that was in contact with the mats, following ISO 10993-5. Briefly, mats were cut into 7 mm diameter disks, sterilized as described previously, placed in wells of a 48-well plate, and covered with 400 µL medium. The medium in wells without mats was also used as a control (Tissue Culture Plate, TCP). They were incubated at 37°C for 4 days, after which the extracts were used to replace the

medium of cells seeded in a 96-well plate at a density of 20,000 cells per well one day prior. After 24h of incubation, the following assays were performed.

3.4.3.1 MTT assay

The MTT assay was conducted to quantify the viability of cells for each condition via metabolic activity. It relies on the reduction of MTT (3-(4,5-dimethylthiazol-2-yl)-2,5-diphenyltetrazoliumbromid) by live cells to formazan crystals, which are dissolved before measuring the optical absorbance, correlating to the number of living cells. For this, the MTT solution is prepared by vortexing MTT powder in PBS at a 5 mg/mL concentration. This solution is sterilized by filtration (pore size < 0,2 µm) and then mixed with DMEM/F12 with a ratio of 1:9. 100 µL of this final solution is added to each well of the 96-well plate in lieu of the medium. The plate is incubated at 37°C for 4h, after which the solution is replaced by 100 µL of DMSO, pipetted to thoroughly dissolve the formazan crystals. The optical absorbance is measured at 570 nm with a microplate reader, and the viability of the cells for each condition is determined by comparing the absorbance to the absorbance of the control, for which the viability is set at 100%.

3.4.3.2 Live/Dead assay

Complementarily, a Live/Dead assay was performed. Here, two dyes are used, one coloring live cells in green and the other coloring dead cells in red. Briefly, cell media is discarded from the wells and cells are gently washed with DPBS two or three times. Then, 100 µL of Live/Dead solution is added (1 µL Calcein-AM and 2 µL EthD-1 in 2 mL DPBS) in each well, and the plate is incubated at 37°C for 30 minutes. The solution is then removed, and the cells are again washed two or three times with DPBS before being imaged with a Leica SP8-DLS confocal microscope.

3.4.4 Initial assessment of cardiomyocyte cultures on electrospun mats

3.4.4.1 Samples preparation and cell seeding

Available electrospun mats were cut into 16 mm diameter samples, sterilized under UV for at least 1h, and placed in a 24-well plate.

Primary ventricular cardiomyocytes (CMs) were harvested and isolated from neonatal Sprague-Dawley rats by other members of the laboratory, following the protocol approved by the Animal Ethics Committee of the Centre Hospitalier Universitaire Sainte-Justine Research Centre (CRCHUSJ, protocol number: 2023-4833). The CMs were used immediately after isolation in Claycomb medium, supplemented with 10% FBS, 1% PS, and 4 mM L-glutamine. 25,000 cells were seeded on each prepared mat in a cloning cylinder (10 mm diameter). 4h after seeding, the cloning cylinders were taken out, and the medium was changed every 2 or 3 days.

3.4.4.2 Cell staining

After 7 days of culture on the mats, cells were stained with Live/Dead dyes as described above, or fixed and stained for specific biomarkers cardiac of Troponin T (cTnT) and F-actin. Briefly, cells on the mats were fixed into a 4 % paraformaldehyde solution for 30 min at room temperature, permeabilized with 0.3 % Triton-X 100 in DPBS for 30 min, and then blocked with a 5 % Bovine Serum Albumin (BSA) and 0.3 % Triton-X 100 solution for 1 h. The solution of primary antibody (cTnT polyclonal antibody) (1:200) was diluted into 1 % BSA in DPBS, which was used to incubate the cells on the mats at 4 °C overnight. They were further covered with a 1 % BSA solution containing secondary antibody Donkey anti-Rabbit Alexa Fluor Plus 488 (1:400) and Phalloidin-iFluor 594 reagent (1:1000) for 1 h. The counterstaining for nuclei was performed with DAPI solution (1:1000) for 20 min, and the mats were then washed 3 times with DPBS before being imaged with either Leica DMi8 wide-field or SP8-DLS confocal microscopes.

3.5 Statistical analysis

Statistical analyses were conducted using GraphPad Prism software. A one-way analysis of variance (ANOVA) followed by Tukey's multiple comparisons post-test was performed to determine the significance of differences between groups (***: $p < 0.001$, **: $p < 0.01$, *: $p < 0.05$). Data are presented as mean ± standard deviation, when applicable. The number of replicates (n) used in the analysis is specified for each experiment.

CHAPTER 4 RESULTS AND DISCUSSION

4.1 Material selection

Electrospinning was employed to produce dense networks of smooth, continuous fibers that were randomly oriented for both Tecoflex™ and Tecophilic™ PU mats, as shown in Figure 4.1. The microstructure of both materials demonstrated the capability to form fibrous mats essential for cardiac patch applications.

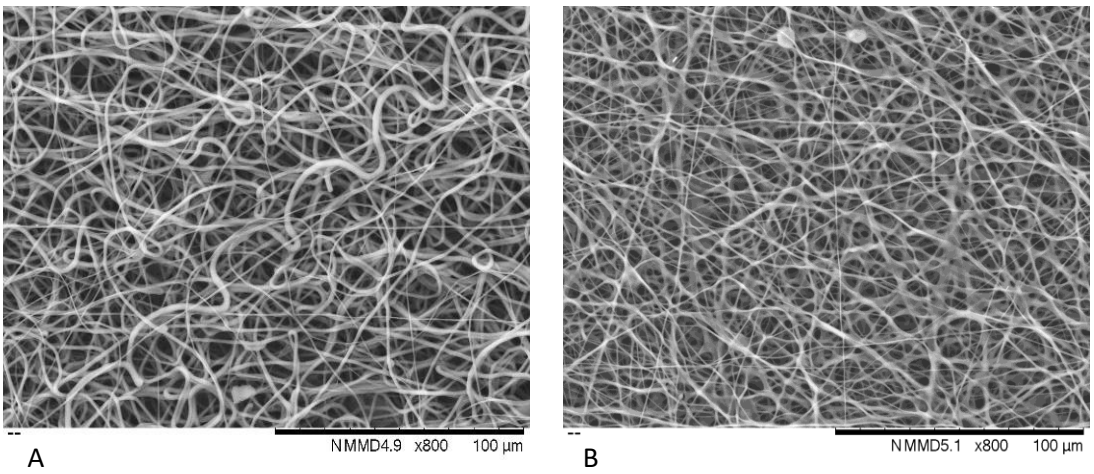

Figure 4.1 : SEM images of Tecoflex™ (A) and Tecophilic™ (B) PU electrospun mats

The mechanical properties of these mats were characterized by tensile testing, with Young's moduli calculated from the linear slope of the stress-strain curves (Figure 4.2). A significant difference was observed between Young's moduli of Tecoflex™ and Tecophilic™ PU mats. Tecoflex™ PU mats exhibited a Young's modulus of 1.11 ± 0.28 MPa, whereas Tecophilic™ PU mats displayed a significantly lower Young's modulus of 0.41 ± 0.13 MPa.

The Young's modulus of Tecophilic™ PU mats is notably closer to that of native myocardium, which ranges from 0.2 to 0.5 MPa during end-diastolic and 0.01 to 0.02 MPa during end-systolic phases [24]. This similarity in mechanical properties justifies the selection of Tecophilic™ PU over Tecoflex™ PU for further development of an electrospun cardiac patch. The mechanical

compatibility of Tecophilic™ PU with native myocardial tissue is critical for ensuring the functional integration and performance of the cardiac patch.

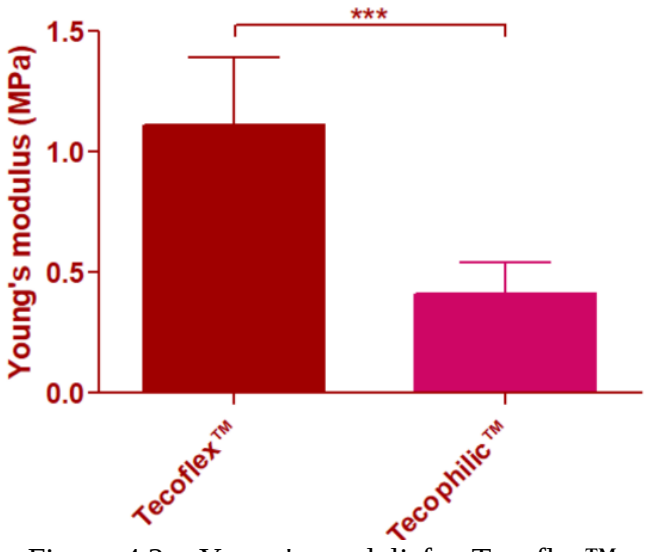

Figure 4.2 : Young's moduli for Tecoflex™ and Tecophilic™ PU electrospun mats. (n=5)

4.2 Fiber characterization

The electrospun mats produced for this study will be referred to by the names detailed in Table 4.1, which describes their composition and fiber orientation.

Table 4.1 : Description of produced electrospun mats

Name	**Composition**	**Fiber orientation**
PU R	Tecophilic™ 5%	Random
PU A	Tecophilic™ 5%	Aligned
PU R-A	Tecophilic™ 5%	Random - Aligned
PU rGO0.5	Tecophilic™ 5% rGO 0.5%	Random - Aligned
PU rGO1	Tecophilic™ 5% rGO 1%	Random - Aligned

The electrospinning process yielded a dense network of continuous fibers, which were predominantly smooth in the mats without rGO (Figure 4.3). Interestingly, fibers produced at higher drum rotation speeds (Figure 4.3 B-C, Figure 4.4 A-C) exhibited slight coiling, likely due to the vertical shrinkage experienced by the mat after being peeled off the aluminum foil. A study showed that CMs cultured on coiled PCL fibers exhibited stronger contraction force, a higher beating rate, and a lower excitation threshold, compared to those cultured on straight fibers [55]. It is argued that straight fibers tend to resist cell movement, limiting contraction potential. In contrast, the coiled fibers move with the cells, reducing mechanical resistance and facilitating stronger and more coordinated contractions across the tissue.

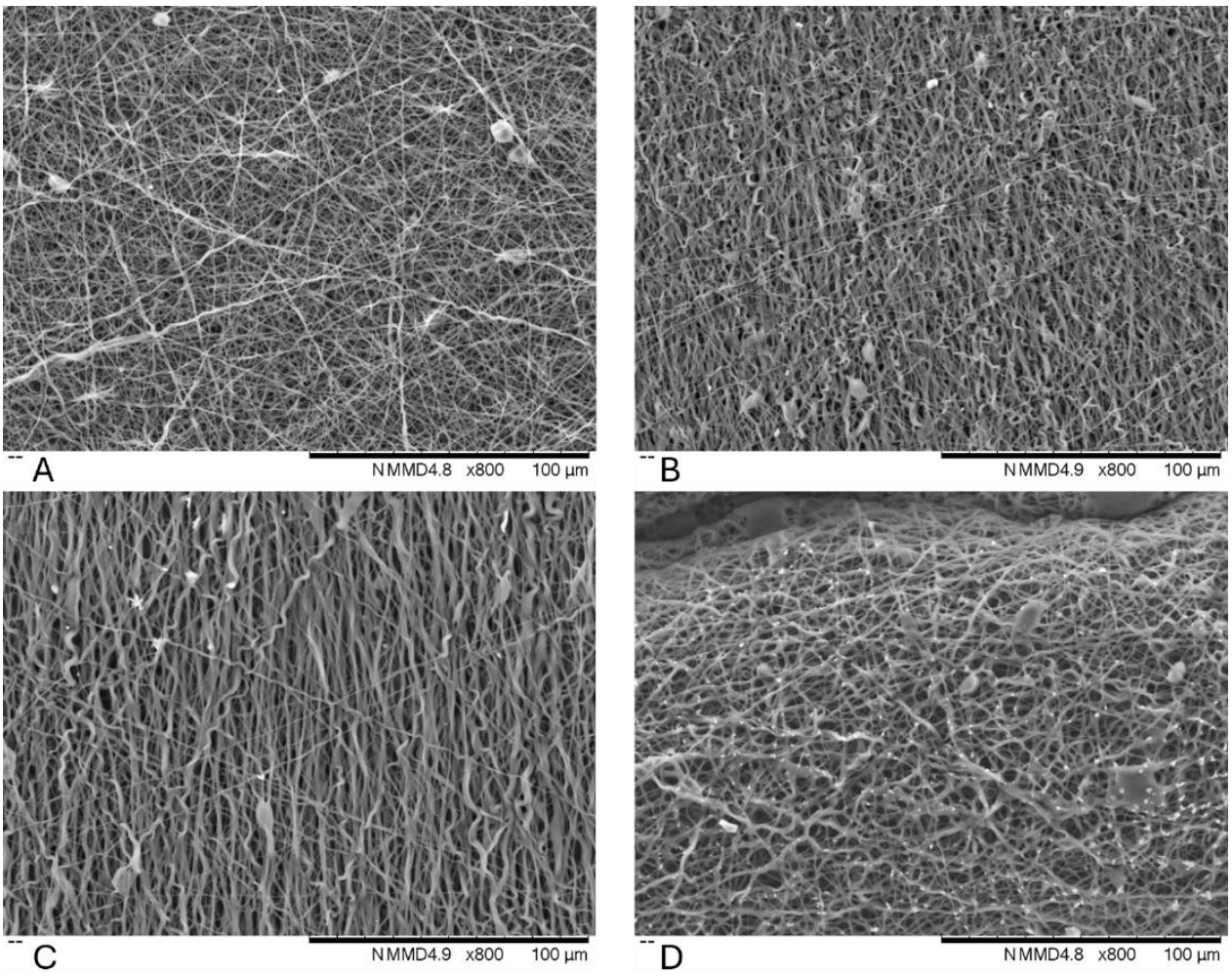

Figure 4.3 : SEM images of mats without rGO. (A) PU R. (B) PU A. (C) PU R-A front side. (D) PU R-A back side.

Mats containing rGO (Figure 4.4) displayed increased surface roughness, with noticeable bead formation around the rGO particles. This roughness is attributed to the presence of rGO, which affects the morphology of the fibers.

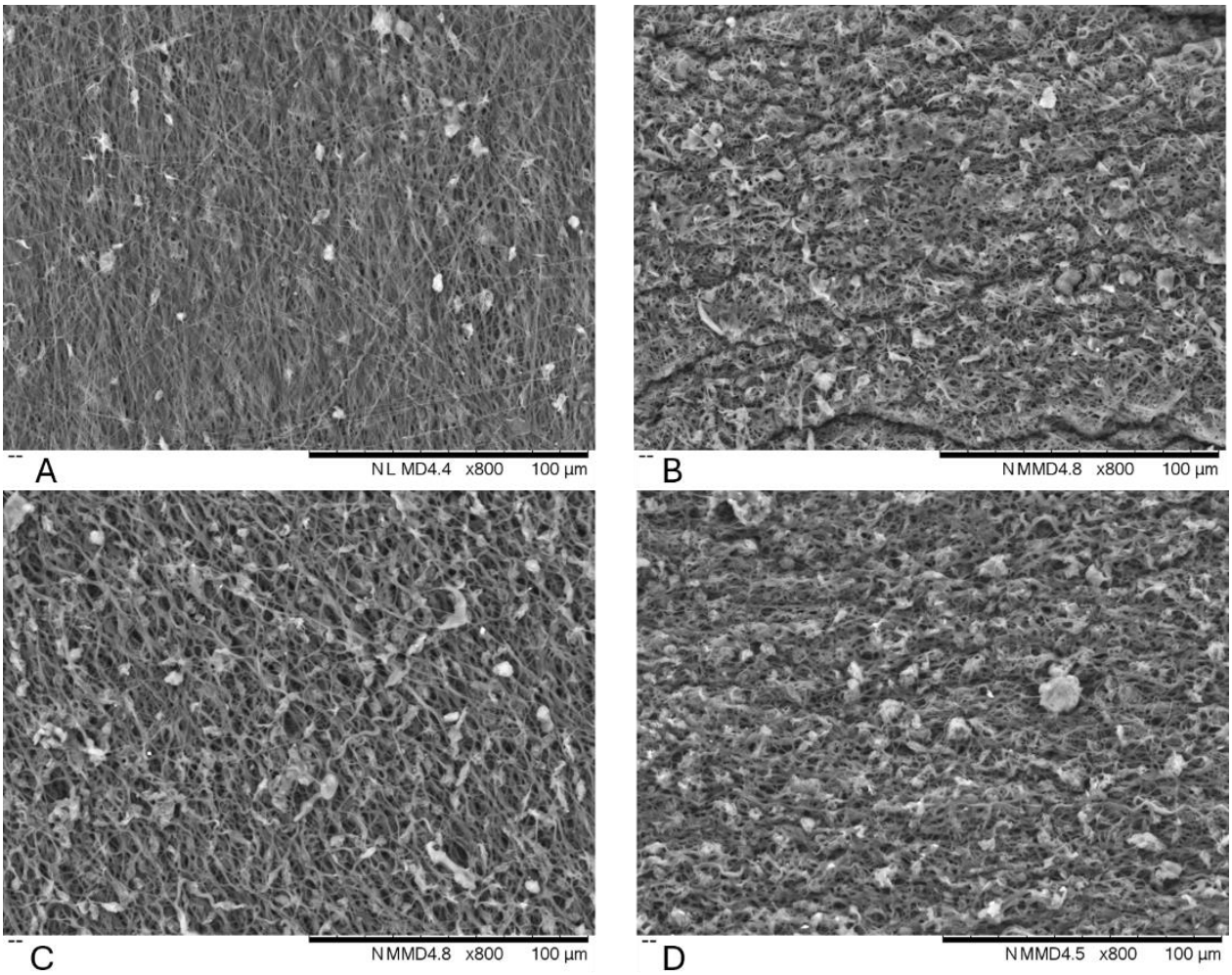

Figure 4.4 : SEM images of mats with rGO. (A) PU rGO0.5 front side. (B) PU rGO0.5 back side. (C) PU rGO1 front side. (D) PU rGO1 back side.

These characterizations highlight the influence of both fiber orientation and rGO addition on the structural properties of the electrospun mats. The smoothness of the fibers in PU R, PU A, and PU R-A mats, combined with the enhanced roughness in PU rGO0.5 and PU rGO1 mats, suggests that the inclusion of rGO significantly modifies the fiber surface, which could impact cell adhesion and mechanical properties.

4.2.1 Diameter

The diameter of the fibers from the produced electrospun mats was analyzed, revealing significant differences based on alignment and the addition of rGO (Figure 4.5).

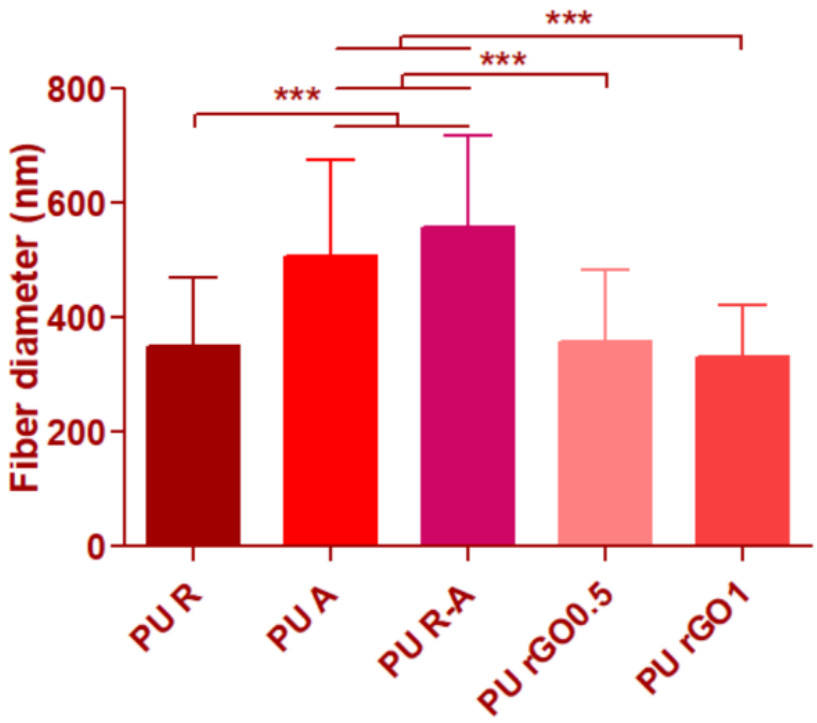

Figure 4.5 : Fiber diameters of produced electrospun mats. (n=100)

Aligned fibers exhibited a notable increase in diameter compared to their randomly oriented counterparts. Specifically, the average diameter for PU R fibers was measured at 349 ± 120 nm. In contrast, PU A and PU R-A fibers displayed significantly larger diameters, measuring 508 ± 167 nm and 559 ± 160 nm, respectively. This increase in fiber diameter could be attributed to a reduced flight time of the fibers due to the higher rotation speed of the collector, therefore reducing the stretching and thinning of the fibers.

The incorporation of rGO into the PU fibers resulted in a substantial reduction in fiber diameter. The average diameter of fibers containing 0.5% rGO decreased to 357 ± 127 nm. Further addition of 1% rGO led to an even more pronounced decrease, with an average diameter of 333 ± 90 nm.

Histograms of fiber diameter distribution for each mat, presented in Appendix A, indicate that the diameters follow a Gaussian distribution. This consistency across samples suggests a uniform effect of alignment and rGO addition on fiber diameter.

The extracellular matrix (ECM) features fibers with diameters of several hundred nanometers [25]. The produced mats replicate these structural properties, thereby facilitating optimal cell-scaffold interactions.

4.2.2 Orientation

The orientation of the fibers from the produced electrospun mats was assessed, and the results are represented in a violin plot (Figure 4.6), showing the fiber orientation distribution for each mat, including the median and quartiles, where 50% of the fibers lie between the first and third quartiles (dashed lines).

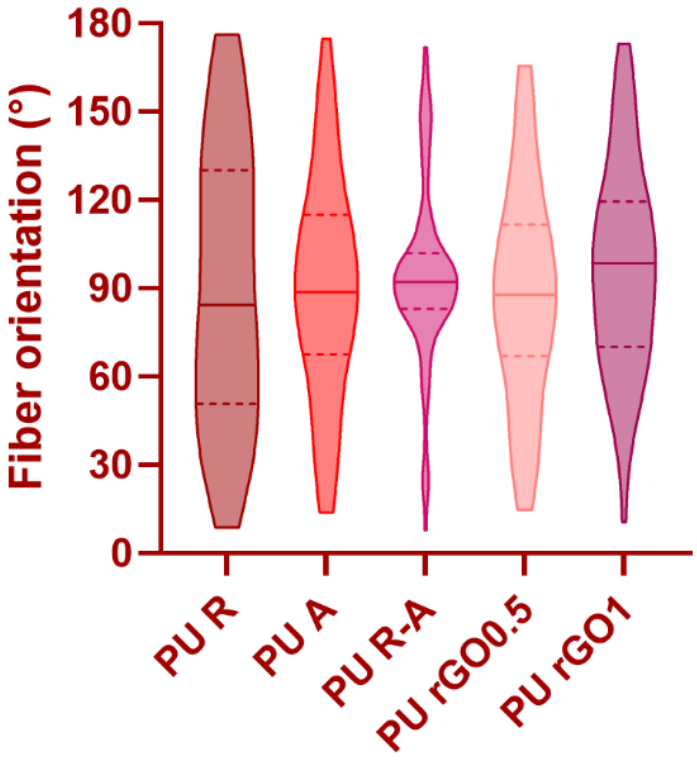

Figure 4.6 : Fiber orientation distributions of produced electrospun mats. Median and quartiles are represented. (n=100)

The orientations are distributed homogeneously for PU R fibers, confirming their random orientation. In contrast, the fiber orientations for the other mats are more concentrated around 90°, indicating a higher degree of alignment.

The fiber orientations in the PU R-A mats are particularly focused around 90°, with 50% of the fibers oriented between 83° and 102°. This high degree of alignment suggests that the presence of randomly oriented fibers at the bottom helps prevent significant shrinkage of the aligned fibers, thereby maintaining their straightness more effectively than in mats composed solely of aligned fibers (PU A).

The addition of rGO appears to produce less aligned fibers compared to the purely PU mats (PU R-A). However, these fibers are still more aligned than those in the PU R mats, which, in contrast, do not follow a Gaussian distribution. Histograms of fiber orientation distribution for each mat, provided in Appendix B, further illustrate these differences.

The violin plots and histograms collectively suggest that while rGO addition slightly reduces fiber alignment compared to PU R-A mats, it still results in a more aligned structure than the random orientation seen in PU R mats, bringing the structure of the mat closer to the native cardiac ECM one. The consistent alignment around 90° in PU R-A underlines the influence of the structural composition on fiber orientation.

4.3 Mats characterization

4.3.1 Mechanical properties

The mechanical properties of the electrospun mats were characterized using stress-strain curves (Figure 4.7), which exhibited two distinct linear slopes for all samples except for PU R. These slopes correspond to the straightening and subsequent elongation of fibers, similar to the stress-strain behavior observed in biological tissues (Figure 4.8) [56]. From these curves, two different elastic moduli (E1 and E2) were determined.

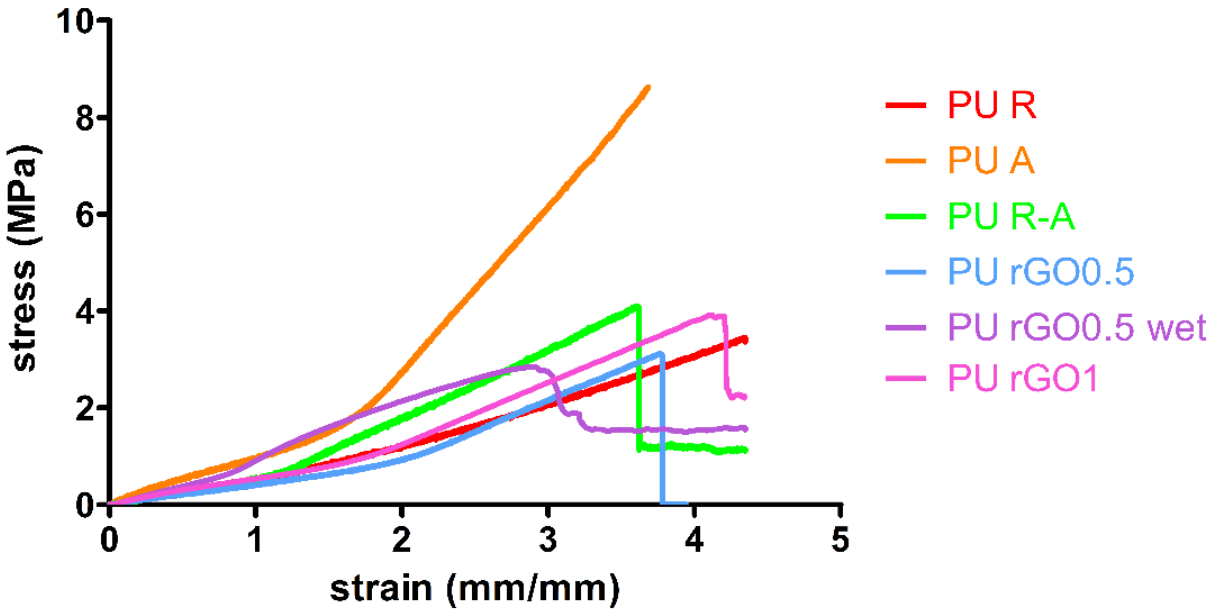

Figure 4.7 : Typical stress-strain curves of electrospun mats from tensile testing

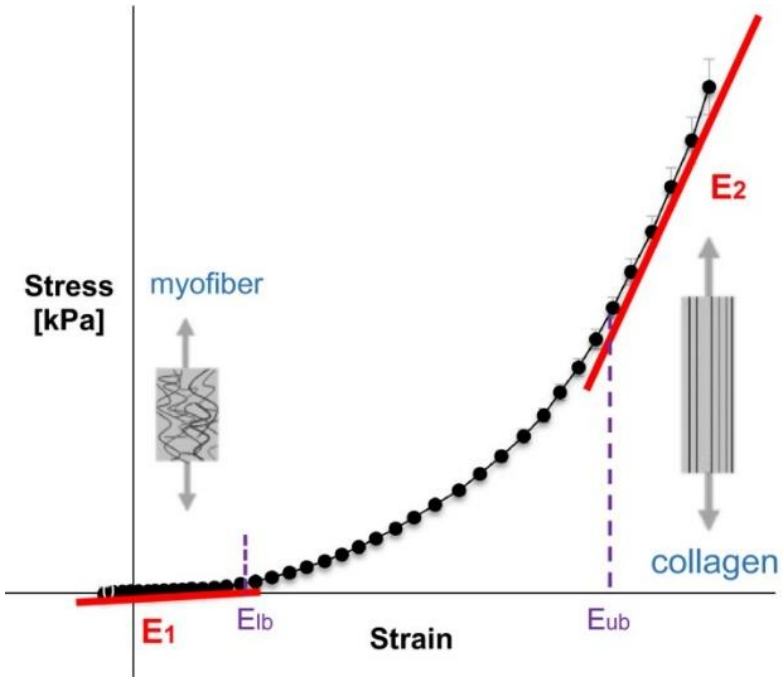

Figure 4.8 : Rat right ventricle myocardium typical tensile stress-strain curve. Reproduced from [56]. © 2017 The Authors. All rights reserved.

PU A mats exhibited the highest values for both elastic moduli, with E1 at 1.19 ± 0.12 MPa and E2 at 3.44 ± 0.68 MPa, significantly higher than those of the other mats containing random or random-aligned fibers (Figure 4.9 A-B). This trend was also observed in the tensile strength (TS), which was 6.96 ± 1.04 MPa for PU A (Figure 4.9 C). The superior mechanical properties of PU A can be attributed to the alignment of the fibers in the testing direction.

In comparison, the mechanical properties of PU R-A mats (E1 = 0.54 ± 0.07 MPa, E2 = 1.34 ± 0.23 MPa, TS = 4.16 ± 0.44 MPa) were closer to those of PU R mats (E1 = 0.58 ± 0.04 MPa, E2 = 0.58 ± 0.04 MPa, TS = 3.98 ± 0.37 MPa). This suggests that the random fibers in the PU R-A mats help mitigate the high modulus and tensile strength imparted by the aligned fibers, keeping the mechanical properties closer to native myocardium values (Young's modulus: 0.2–0.5 MPa end-diastolic, 0.01–0.02 MPa end-systolic; Tensile strength: 3–15 kPa [24]). Therefore, those mats achieve adequate mechanical properties for cardiac tissue engineering, while presenting with aligned fibers at their surface, which is beneficial for cell alignment.

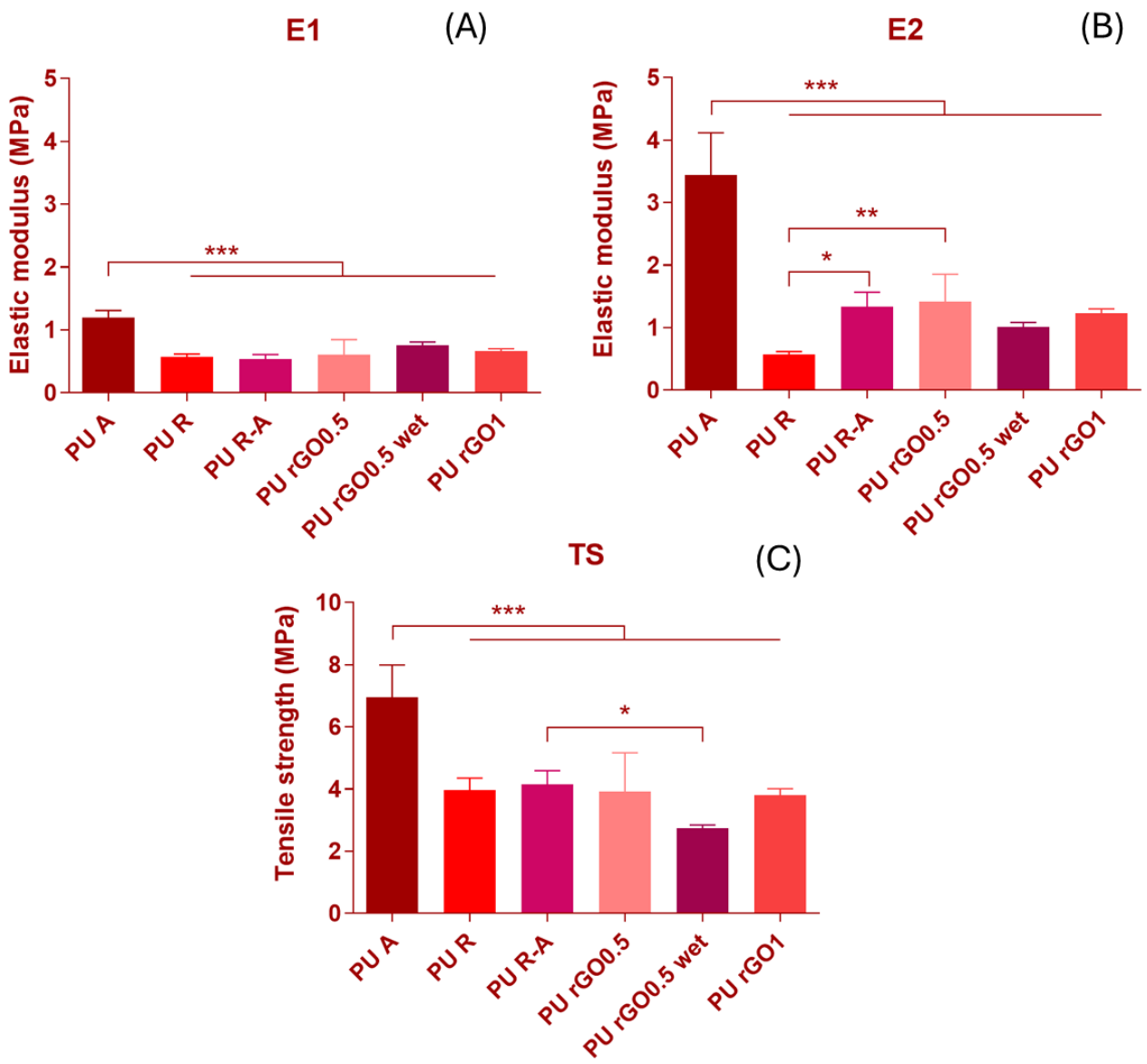

Figure 4.9 : Mechanical properties of electrospun mats. (n=5). (A) First elastic moduli E1. (B) Second elastic moduli E2. (C) Tensile strength.

The addition of rGO at both concentrations did not significantly affect the mechanical properties, staying in the range of PU R-A ones.

Wetting the mats did not significantly alter their mechanical properties overall, though the tensile strength and E2 of the wet mats were lower than those of the dry mats (PU rGO0.5). Specifically, the tensile strength decreased from 3.92 ± 1.25 MPa to 2.74 ± 0.11 MPa, and E2 decreased from 1.42 ± 0.44 MPa to 1.01 ± 0.07 MPa. This decrease can be attributed to the adsorbed water breaking hydrogen bonds within the mat [57].

Elongation at break was not reported, as the axis limit of the testing machine was often reached before the mats broke. However, elongation at the final point or at break consistently exceeded 300% for every mat, which is sufficient to accommodate the stretch caused by heart contraction and relaxation (between 20 and 30% [11]).

The mechanical properties values of each mat are summarized in Table 4.2.

Table 4.2 : Mechanical properties of produced electrospun mats

	E1 (MPa)	**E2 (MPa)**	**TS (MPa)**
PU A	1.19 ± 0.12	3.44 ± 0.68	6.96 ± 1.04
PU R	0.58 ± 0.04	0.58 ± 0.04	3.98 ± 0.37
PU R-A	0.54 ± 0.07	1.34 ± 0.23	4.16 ± 0.44
PU rGO0.5	0.61 ± 0.23	1.42 ± 0.44	3.92 ± 1.25
PU rGO0.5 wet	0.75 ± 0.06	1.01 ± 0.07	2.74 ± 0.11
PU rGO1	0.67 ± 0.03	1.23 ± 0.07	3.80 ± 0.21

4.3.2 Conductivity

Electrical conductivity ensures that cardiac patches can synchronize with the natural electrical impulses of the heart, facilitating coordinated contractions and effective pumping. The volume conductivity of the electrospun mats exhibited a marked increase with the incorporation of rGO (Figure 4.10). Pure PU mats displayed a conductivity of 1.1 ± 0.2 $\times 10^{-8}$ mS/cm. When rGO was added at a concentration of 0.5%, the conductivity increased to 3.2 ± 0.3 $\times 10^{-7}$ mS/cm. Further increasing the rGO concentration to 1% resulted in a conductivity of 2.1 ± 0.9 $\times 10^{-6}$ mS/cm, significantly different than PU and PU rGO0.5 mats.

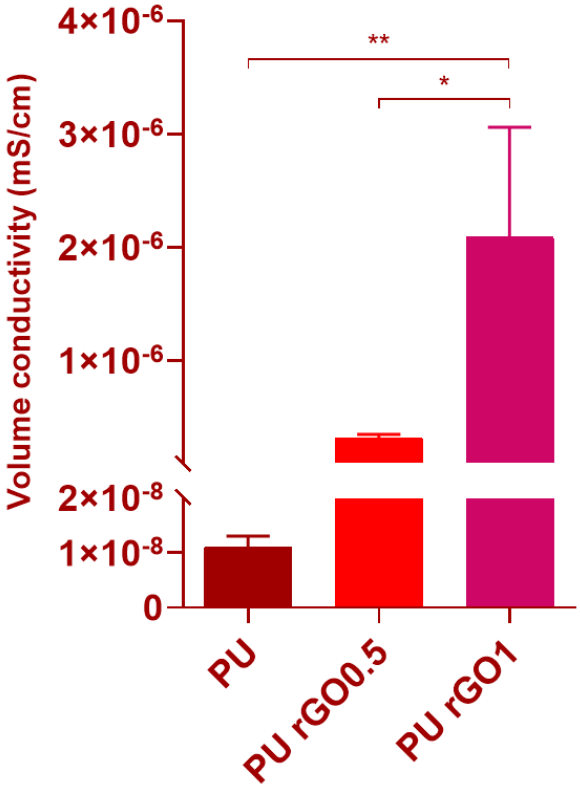

Figure 4.10 : Volume conductivity of electrospun mats with and without rGO. (n=3)

Although the conductivity of the rGO-enhanced mats remains substantially lower than that of native myocardium (with reported effective extracellular longitudinal and transverse conductivities of 2.1 mS/cm and 0.5 mS/cm, respectively [26]), it is important to consider the potential impact of a wet environment. The presence of ions in the medium, with an extracellular electrolyte

conductivity of 20 mS/cm [26], suggests that the actual conductivity in physiological conditions would be higher, however, the equipment used only allows testing in dry conditions.

Therefore, the addition of rGO to the electrospun mats can be presumed to facilitate electrical signaling between cells, as previously demonstrated [33], [40], thereby enhancing their potential for use in cardiac tissue engineering applications.

4.3.3 Coating chemical composition

The chemical composition of the plasma-polymerized coating applied to the electrospun fibers to enhance their cell adhesion properties was analyzed using XPS. The analysis focused on the relative atomic percentage of nitrogen present in the samples, aiming to assess the effectiveness of the nitrogen-rich coating.

For the PU rGO0.5 mat, the nitrogen content was found to be relatively low, with a nitrogen atomic percentage of 0.7%. However, nitrogen content was substantially increased after applying the nitrogen-rich plasma-polymerized coating (LPPE:N) to the PU rGO0.5 mat, with [N] rising to 17.8%.

This notable increase in nitrogen content confirms the successful deposition of the nitrogen-rich plasma-polymerized coating on the electrospun fibers. The observed nitrogen content is of the same order of magnitude as reported in a previous study, where the same coating was applied to PET electrospun fibers, resulting in a [N] of 13% [47].

The presence of this coating is expected to enhance cell adhesion and proliferation, owing to the improved surface chemistry provided by the increased nitrogen content (specifically primary amines) [47], [51].

4.4 *In vitro* testing

4.4.1 Indirect cytotoxicity assessment

1.4.1.1 MTT assay

The indirect cytotoxicity of the electrospun mats was evaluated using the MTT assay, which measures cell viability in comparison to the TCP control. Overall, the results indicated good viability across the different mats (Figure 4.11).

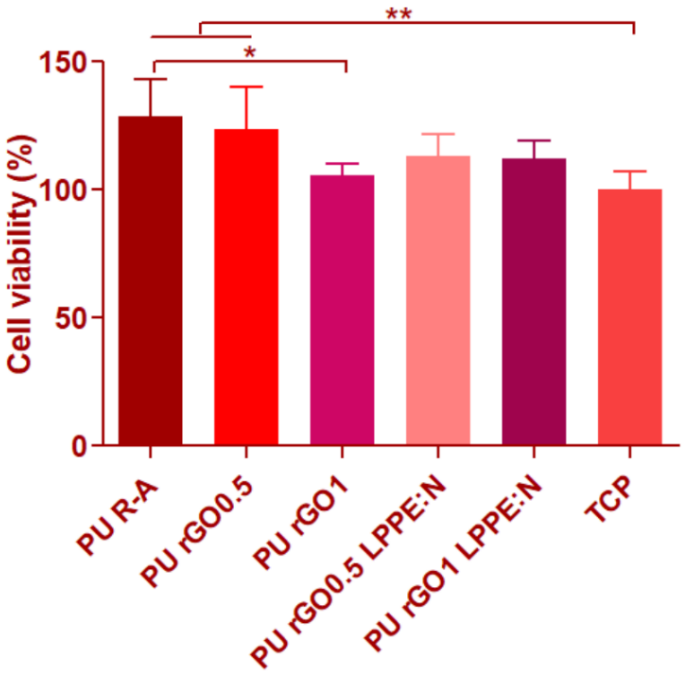

Figure 4.11 : Cell viability evaluated via MTT reduction in indirect cytotoxicity assessment of electrospun mats, normalized to TCP control. (n=6)

Cells cultured in the PU R-A mat extract exhibited the highest viability, at 128 ± 15%. This was closely followed by cells cultured in the PU rGO0.5 extract, with a viability of 123 ± 17%. While cells cultured in the PU rGO1 extract showed a significant decrease in viability compared to those in the PU R-A extract, their viability was still higher than the TCP control, at 105 ± 6%.

Extracts from the coated mats, PU rGO0.5 LPPE:N and PU rGO1 LPPE:N, showed similar viabilities of 113 ± 8% and 112 ± 7%, respectively. These values indicate an improvement in cell viability compared to the uncoated PU rGO1 extract.

Although the MTT assay approximates metabolic activity to viability, these results should not be interpreted as an indication that the mats enhance cell proliferation, as increased metabolic activity can also result from cellular stress [58]. Nonetheless, the results confirm that the produced electrospun mats do not provoke cytotoxicity indirectly.

4.4.1.2 Live/Dead

Complementary to the MTT assay, Live/Dead staining was performed to assess indirect cytotoxicity. The Live/Dead images corroborate the MTT results, demonstrating good viability across all conditions (over 90%), with very few red-stained cells indicating cell death (Figure 4.12). Most cardiac fibroblasts exhibited a spindle-like morphology, which is characteristic of their native phenotype. Table C.1 summarizing values of cell counting can be found in Appendix C.

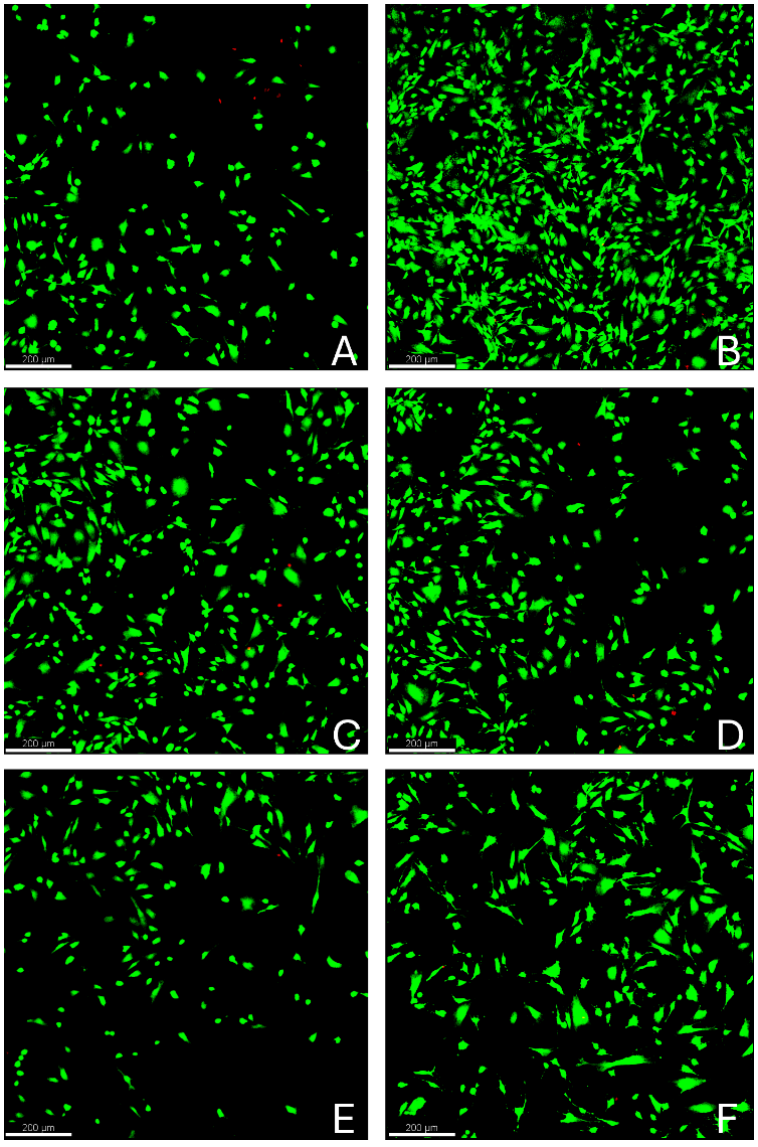

Figure 4.12 : Live/Dead staining images resulting from indirect cytotoxicity assessment of electrospun mats. (A) TCP control. (B) PU R-A mat. (C) PU rGO0.5 mat. (D) PU rGO0.5 LPPE:N mat. (E) PU rGO1 mat. (F) PU rGO1 LPPE:N mat.

In agreement with the MTT results, a higher number of cells was observed when cultured in the PU R-A mat extract (Figure 4.12 B). Conversely, fewer cells were seen when cultured in the PU rGO1 mat extract (Figure 4.12 E), although the cell count was similar to that of the TCP control (Figure 4.12 A). Additionally, an increased number of cells was observed in the extracts from mats with the LPPE:N coating (Figure 4.12 D and F), compared to those cultured in the PU rGO1 mat extract, with a cell count similar to that seen in the PU rGO0.5 mat extract (Figure 4.12 C).

These findings reinforce the conclusions drawn from the MTT assay, confirming that the produced electrospun mats do not exhibit indirect cytotoxicity.

4.4.2 Preliminary evaluation of cardiomyocyte viability and phenotype

Figure 4.13 presents partial results from a preliminary study with CM culture on the produced mats, featuring immunostaining images in the first row (A-C) and Live/Dead staining images in the second row (D-F).

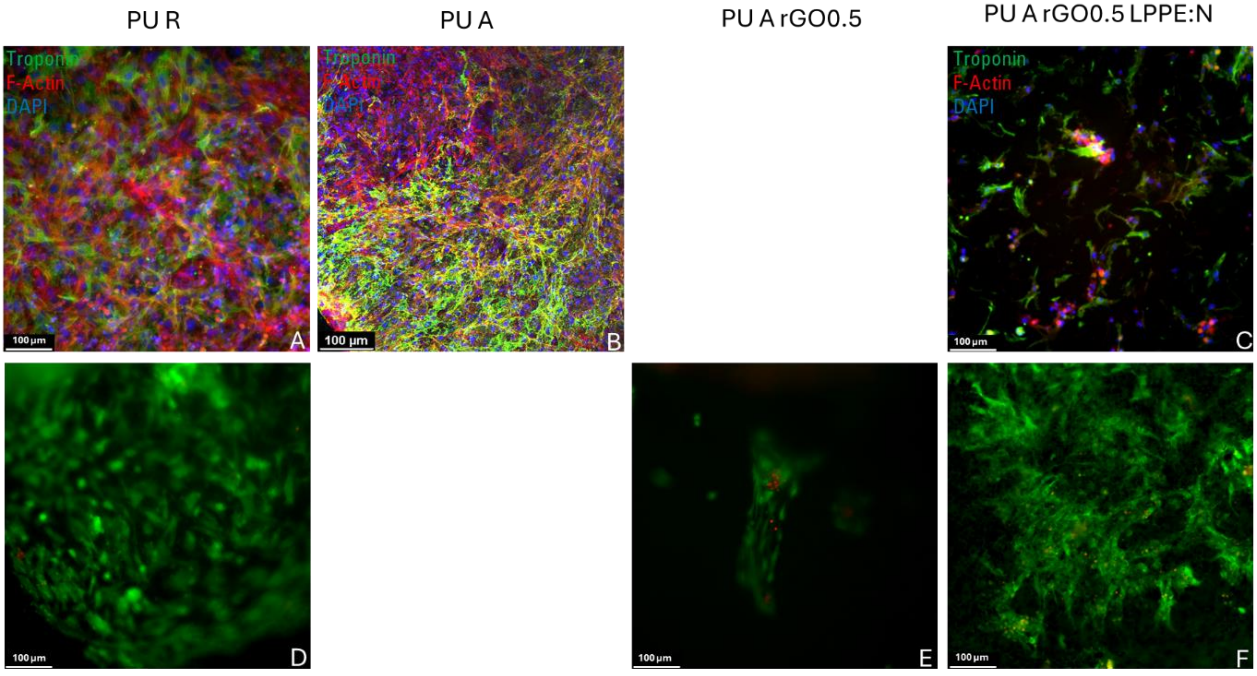

Figure 4.13 : Microscopy images from CMs culture on electrospun mats. (A-C) Immunostaining images showing troponin (green), f-actin (red), DAPI (blue), on PU R mat (A), PU A mat (B), and PU A rGO0.5 LPPE:N mat (C). (D-F) Live/Dead staining images of cells on PU R mat (D), PU A rGO0.5 mat (E), and PU A rGO0.5 LPPE:N (F).

Due to issues with mats rolling onto themselves during cell culture, information could not be collected for all mats tested. Despite these challenges, some insights were obtained :

- **PU R Mat**: Cells cultured on the PU R mat exhibited good viability, as evidenced by the Live/Dead staining (Figure 4.13 D). The immunostaining images (Figure 4.13 A) showed a uniform presence of specific cardiac biomarkers troponin and f-actin, indicating a healthy CM phenotype.
- **PU A Mat**: Similar to the PU R mat, cells cultured on the PU A mat displayed a consistent presence of cardiac biomarkers (Figure 4.13 B), suggesting good viability.
- **PU rGO Mat**: The addition of rGO appeared to reduce cell viability, as indicated by increased red-stained (dead) cells in the Live/Dead image and generally fewer cells (Figure 4.13 E). This suggests a potential negative impact of rGO on CM viability.
- **PU rGO with LPPE:N Coating**: The application of the LPPE:N coating visibly improved cell viability (Figure 4.13 F). However, this observation was contradicted by the immunostaining results, which showed fewer cells and less defined cardiac biomarker structures (Figure 4.13 C).

These preliminary findings highlight the need for further exploration of cellular adhesion, proliferation, and phenotype on these electrospun mats. While promising results were observed, particularly with the PU R and PU A mats, the effects of rGO and the LPPE:N coating require more detailed investigation to fully understand their impact on CM behavior.

CHAPTER 5 GENERAL DISCUSSION

This research project focused on developing a biocompatible and conductive electrospun patch for cardiac tissue regeneration, addressing several critical aspects of material science and bioengineering. This discussion will elaborate on the significant areas covered in the research, including material selection, fabrication techniques, characterization, and *in vitro* testing, as well as highlight potential areas for future exploration.

5.1 Material selection and fabrication

Within the scope of this study, PU was selected as the primary material for electrospinning due to its favorable mechanical properties, biocompatibility, and elasticity. Two types of medical-grade PUs, Tecoflex™ and Tecophilic™, were evaluated for their suitability in cardiac tissue engineering. Tecophilic™ PU was chosen for further development based on its mechanical properties, which closely resemble those of native myocardial tissue.

The incorporation of rGO into PU fibers aimed to enhance the electrical conductivity of the patches. The study demonstrated that the addition of rGO significantly improved the conductivity of the electrospun mats, although the values remained lower than those of native myocardium. Future work could focus on optimizing the rGO concentration and exploring alternative dispersion or incorporation techniques to achieve more uniform distribution and higher conductivity.

As a substitute for simply dispersing rGO into the electrospinning solution, rGO can be electrosprayed in parallel to the electrospinning process. Electrospraying involves a similar principle as electrospinning but creates fine droplets from a solution instead of a jet. One study simultaneously used this technique with the electrospinning of PU to incorporate rGO into nanofibrous scaffolds [59]. The results showed that the electrical conductivity of the PU/rGO composite significantly improved with increasing concentrations of electrosprayed rGO. Specifically, the scaffold containing 15% rGO (relative to PU weight) reached the percolation threshold, with a conductivity of 3.46×10^{-5} S/cm. The highest conductivity was observed in the scaffold with 20% rGO, reaching 6.05×10^{-5} S/cm, while the one with 10% rGO had a conductivity

of only 2.13×10^{-11} S/cm. They also investigated the electrical conductivity of an electrospun scaffold prepared from the blend of PU with 20% rGO, measured at only 8.19×10^{-12} S/cm, which is nearly the same as the pure PU scaffold (5.84×10^{-12} S/cm). The concentrations of rGO incorporated into the electrospinning solution in this present study (0.5 and 1%) correspond to 10 and 20% of PU's weight, respectively. The results from both studies can therefore be compared, depending on the rGO concentrations and the two different incorporation methods used (Table 5.1).

Table 5.1 : Comparison of electrical conductivities (S/cm) measured in [59] and this study for different rGO concentrations and incorporation methods.

Measured in :	**Pure PU**	**rGO: 10% of PU's weight electrosprayed**	**rGO: 10% of PU's weight blended**	**rGO: 20% of PU's weight electrosprayed**	**rGO: 20% of PU's weight blended**
Article [59]	5.84×10^{-12}	2.13×10^{-11}	-	6.05×10^{-5}	8.19×10^{-12}
This study	$1.1 \pm 0.2 \times 10^{-11}$	-	$3.2 \pm 0.3 \times 10^{-10}$	-	$2.1 \pm 0.9 \times 10^{-9}$

Even at the same rGO concentration and incorporation method (20% of PU's weight blended), the conductivities measured in both studies are notably different, with a value 256 times higher measured here. This can be due to various factors, like a different conductivity measurement technique used (four-point probe method in [59] versus parallel electrodes), different fiber morphologies, different types of PU used (Tecoflex SG-80A in [59], less hydrophilic than Tecophilic), different rGO dispersions in the blend. This difference aside, it is still evident that electrospraying of rGO leads to significantly higher electrical conductivity than simply blending, at a specific concentration threshold. It is suggested that this is due to the entrapment of rGO particles within the insulating PU fibers when blending, preventing the formation of conductive pathways, which are crucial for achieving high conductivity [59]. In contrast, the method of electrospraying rGO onto the electrospun PU fibers allowed the rGO to be more uniformly distributed on the surface of the fibers and within the scaffold, leading to significantly higher electrical conductivity. Adopting this method in future work could not only contribute to achieving higher electrical conductivity at lower rGO concentrations but also help to obtain a better fiber

alignment, as the instability in the electrospinning jet due to rGO conductive particles presence would be eliminated.

5.2 Characterization of electrospun mats

The electrospun mats were characterized for their fiber morphology, mechanical properties, and electrical conductivity. SEM revealed smooth, continuous fibers with increased roughness and bead formation upon rGO addition. Mechanical testing showed that PU mats with random and aligned fibers exhibited properties closer to the native myocardium, making them suitable for cardiac patches, while presenting with fiber alignment at the surface.

Table 5.2 presents a summary of the mechanical and electrical properties, along with the composition, of the electrospun patches developed in this study (PU rGO1%), compared to those from aforementioned studies. Among the studies compared, our patch exhibits one of the lowest Young's modulus, the lowest tensile strength, and the highest elongation at break. These characteristics align it more closely with the mechanical properties of native myocardium, making it highly adaptable to the cyclic stretching caused by heart contraction and relaxation. However, it shows the lowest conductivity, as previously discussed.

Table 5.2 : Comparison of mechanical and electrical properties of electrospun cardiac patches with this study

Cardiac patch composition	**Young's modulus (MPa)**	**Tensile strength (MPa)**	**Elongation at break (%)**	**Conductivity (mS/cm)**
This study: PU /rGO	0.67 ± 0.03	3.80 ± 0.21	> 300	$2.1 \pm 0.9 \times 10^{-6}$
[59]: PU / rGO	41.76 ± 0.66	34.81 ± 4.14	115.01 ± 1.36	6.05×10^{-2}
[42]: PANi / hyaluronic acid / collagen	2 ± 1 (dry); 0.02 ± 0.01 (wet)	9.3 ± 0.5 (dry); 4 ± 2 (wet)	2.2 ± 0.9 (dry); 78 ± 8 (wet)	2.0 ± 0.6

Table 5.2 : Comparison of mechanical and electrical properties of electrospun cardiac patches with this study (continued)

Cardiac patch composition	**Young's modulus (MPa)**	**Tensile strength (MPa)**	**Elongation at break (%)**	**Conductivity (mS/cm)**
[43]: PVA / chitosan / PEDOT:PSS	-	18.78 ± 0.95	5.6 ± 0.3	7.63×10^{-2}
[34]: PU / CNT	2.32	3 ± 23.63	62.64 ± 7	$5.46 \pm 0.01 \times 10^{-2}$

A missing part of the characterization work is the degradability assessment of the mats in physiological conditions, an important parameter to consider to ensure good integration with the native tissue and optimal tissue regeneration. PU must degrade at a rate that matches the tissue regeneration timeline, ensuring that the patch provides support during the initial healing phase and gradually transfers the load to the newly formed tissue. Tecophilic is a hydrophilic polyether-based thermoplastic aliphatic PU, a type of PU being known to degrade via hydrolysis of their urethane groups or via oxidation of the aliphatic fragments carrying ether bonds (R-O-R') [60], [61].

One study developed Tecophilic/Gelatin nanofibers for small-diameter blood vessel tissue engineering and discussed their *in vitro* degradation in incubation in PBS [60]. The study reveals that Tecophilic, when combined with gelatin, exhibits significant swelling and gradual mass loss over time. The mass loss of the composite scaffold increased from 16.9% after 7 days to 25.7% after 28 days, indicating that it degrades slowly but steadily in a hydrated environment. However, pure Tecophilic fibers did not show any mass loss over this period of time. The study suggests that while Tecophilic itself is highly resistant to degradation in purely aqueous environments (like PBS), the degradation process might be significantly influenced by the direct interaction with cells, which could initiate degradation by oxidative mechanisms. The proposed mechanism involves cells, particularly phagocytic cells, releasing reactive oxygen species (ROS) and other oxidative agents such as hydrogen ions and enzymes. These agents are capable of attacking the polymer chains of Tecophilic, specifically its ether bonds, leading to its gradual breakdown. The presence of cells could thus accelerate the degradation process, potentially leading to a faster mass loss of the material than what is observed in purely *in vitro* conditions without cellular presence.

Another study explored the *in vivo* degradation of Tecoflex EG-80A, a PU from the same family, used in the production of electrospun vascular grafts in combination with gelatin [61]. The study found that Tecoflex exhibits some degree of degradation when implanted in rats, specifically a reduction in molecular weight by approximately 10% after 3 months. Despite this degradation, the tensile strength of the grafts only decreased initially but later increased after 6 months, suggesting a recovery or adaptation phase, possibly due to tissue ingrowth stabilizing the material. Although Tecoflex shows signs of degradation through hydrolysis and oxidation, its mechanical properties demonstrate resilience, which might support the gradual transfer of load to newly formed tissue during the healing process.

The results from these studies support the idea that Tecophilic scaffolds, when used in tissue engineering applications, could degrade in a controlled and biologically responsive manner, which is crucial for optimal tissue integration and regeneration. One remaining interrogation is the influence of rGO incorporation and LPPE:N coating on the degradation rate of the mats, which should be studied in future works.

5.3 Plasma-polymerized coatings

To enhance cell adhesion, a nitrogen-rich plasma-polymerized coating (LPPE:N) was applied to the electrospun mats. XPS confirmed a substantial increase in nitrogen content, indicating successful coating deposition. The presence of this coating is expected to improve cell adhesion due to the enhanced surface chemistry. LPPE:N indeed possesses primary amine ($–NH_2$) groups, which in aqueous solutions at physiological pH values hold a localized positive charge, believed to attract the negatively charged biomolecules (proteins) and cells [47], [49].

This was not shown evidently in the preliminary evaluation conducted with CMs. Admittedly their viability and adhesion seemed improved with LPPE:N compared to PU/rGO fibers without coating. However, the immunostaining only showed dispersed cells with disorganized biomarker structures, in contrast to the numerous CMs that exhibit specific biomarkers uniformly on PU-only fibers (Figure 4.13). However, the limited amount of data collected does not allow for conclusions to be drawn, and further studies are required. Specifically, quantification of primary amine groups

introduced via LPPE:N coating could determine if their concentration is sufficient. This can be done by 4-trifluoromethyl-benzaldehyde (TFBA) derivatization, where TFBA molecules are chemically grafted to the primary amines before XPS analysis, fluorine concentration detected corresponding to primary amines concentration [45]. In this previously referenced study applying LPPE:N coatings on PET fibers and proving their enhanced adhesion properties for HUVECs, [NH_2] was measured to be around 6 at.% [47].

If it transpires that LPPE:N does not sufficiently promote the adhesion of CMs, other plasma-polymerized coatings could be explored. For example, one study investigated the use of plasma-polymerized oxygen-functional hydrocarbon coatings on electrospun PCL fibers [62]. These coatings were created through the feeding of ethylene, carbon dioxide and argon gases into a vacuum chamber, where the pressure was 0.1 mbar and the RF power input 34W. The plasma-coated substrates demonstrated enhanced muscle cell adhesion, proliferation, and differentiation compared to uncoated substrates. Specifically, these coatings promoted the formation of myotubes with higher density, alignment, and contractility, which are crucial properties for the development of functional muscle tissues. The proposed mechanism to explain the improved cellular adhesion is similar to the one for nitrogen-rich coatings: carbonyl, carboxyl and hydroxyl groups generated by the oxygen-functional hydrocarbon coating, negatively charged, increased protein adsorption and resultant cell retention. These findings with muscle cells suggest that this plasma-polymerized oxygen-functional hydrocarbon coating could be a promising candidate for further studies with CMs.

Plasma-polymerized coatings with grafted bioactive molecules could also be explored in future studies, to further improve the biocompatibility and therapeutic efficacy of the patches. The grafting of immunomodulatory molecules would be particularly interesting, in order to address the issue of possible adverse immune response affecting the cardiac patches' properties, and effectively guide the native tissue toward regeneration.

While the effect of LPPE:N coating on the mechanical properties of the coated mats was not tested, a past study did not observe significant differences between coated and uncoated PET fibers when tested wet [47]. Regarding its effect on electrical conductivity, although it has not been directly investigated, the presence of negatively charged primary amines suggests a potential enhancement of conductivity, a possibility to be explored in future studies.

5.4 *In vitro* testing

In vitro testing included indirect cytotoxicity assessment using MTT and Live/Dead assays, which indicated good cell viability and no significant cytotoxicity. Primary CMs were cultured on the electrospun mats to evaluate their biocompatibility and support for cell growth.

In order to address the issue of electrospun mats rolling onto themselves observed during this preliminary experiment, a specific culture technique was developed. Mats were cut into 9 mm diameter disks, wetted in PBS to let them swell, and subsequently glued to 12 mm diameter glass coverslips, by application of less than 5 µL Eukitt mounting medium around the edge of the coverslips. 10 mm diameter glass cloning cylinders were laid on top of the glued mats, which were left under the hood for at least 24h to wait for the complete drying of the glue. LPPE:N coatings were deposited at this point, followed by sterilization in an antibiotic solution and under UV for at least 90 minutes. Cell culture can then be performed in 24-well plates, leaving cloning cylinders on top of the mats during the entire culture duration to prevent them from detaching from the glass coverslips. After staining, coverslips can be carefully taken out of the wells and reversed into glass bottom microscopy dishes for imaging.

Future research could involve more extensive *in vitro* testing using this culture technique and later *in vivo* testing to assess the long-term biocompatibility, integration with native tissue, and functional performance of the patches. Investigating the immune response and potential inflammatory effects *in vivo* will be crucial for clinical translation.

CHAPTER 6 CONCLUSION AND RECOMMENDATIONS

This research aimed to develop and characterize a biocompatible and conductive electrospun patch for cardiac tissue engineering that closely replicates the structural, mechanical, and electrical properties of the native myocardium. The study successfully fabricated electrospun mats using medical-grade PU, specifically Tecophilic™ SP-80A-150 PU, selected for its mechanical properties that align closely with those of native cardiac tissue. The Young's modulus of the Tecophilic™ PU mats was measured at 0.41 ± 0.13 MPa, which is within the range of native myocardium (0.2–0.5 MPa during diastole), justifying its selection for further development.

To enhance electrical conductivity, rGO was incorporated into the PU fibers at concentrations of 0.5% and 1%. The addition of 1% rGO resulted in a significant increase in conductivity, reaching $2.1 \pm 0.9 \times 10^{-6}$ mS/cm, compared to $1.1 \pm 0.2 \times 10^{-8}$ mS/cm for the pure PU mats. Although this conductivity is still below the effective extracellular conductivity of native myocardium (2.1 mS/cm longitudinally and 0.5 mS/cm transversely), the presence of rGO significantly improved the electrospun mats' electrical properties.

The mechanical characterization revealed that the mats with aligned fibers (PU A) exhibited superior mechanical properties, with an E1 of 1.19 ± 0.12 MPa and a tensile strength of 6.96 ± 1.04 MPa. However, mats with both random and aligned fibers (PU R-A) presented more balanced properties, with an E1 of 0.54 ± 0.07 MPa, E2 of 1.34 ± 0.23 MPa, and tensile strength of 4.16 ± 0.44 MPa. These values suggest that the PU R-A mats better replicate the mechanical environment of the native myocardium, which undergoes significant mechanical strain during the cardiac cycle.

Additionally, the application of a nitrogen-rich plasma-polymerized coating (LPPE:N) aimed to improve cell adhesion on the mats. Initial *in vitro* testing using CMs was inconclusive regarding its effect on cell adhesion, and further study and optimization are needed to fully realize its potential. Specifically, the cell viability on coated mats was slightly lower than expected, indicating that the interaction between the coating and the rGO-modified fibers may require further adjustment.

In vitro cytotoxicity assessments confirmed the biocompatibility of the developed mats, with MTT assay results showing cell viability rates of over 100% in the presence of all mats extract. The Live/Dead staining also supported these findings, with a majority of cells appearing viable.

In summary, this study successfully demonstrated the potential of electrospun PU/rGO mats as cardiac patches, showing promising mechanical and electrical properties. However, achieving the full integration of these patches into cardiac tissue will require further refinement, particularly in optimizing the balance between mechanical strength, electrical conductivity, and cell compatibility. Future work should focus on improving the electroconductivity and the bioactivity of the mats, possibly through the incorporation of additional bioactive molecules or by further fine-tuning the plasma polymerization process. These efforts could lead to the development of more effective therapies for cardiac tissue regeneration, addressing the urgent need for innovative solutions in the treatment of CVDs.

REFERENCES

[1] "Cardiovascular diseases (CVDs)," World Health Organization. Accessed: Aug. 01, 2024. [Online]. Available: https://www.who.int/news-room/fact-sheets/detail/cardiovascular-diseases-(cvds)

[2] P. H. A. of Canada, "Heart Disease in Canada." Accessed: Nov. 17, 2023. [Online]. Available: https://www.canada.ca/en/public-health/services/publications/diseases-conditions/heart-disease-canada.html

[3] WHO's Global Health Estimates, "The top 10 causes of death," World Health Organization. Accessed: Aug. 04, 2024. [Online]. Available: https://www.who.int/news-room/fact-sheets/detail/the-top-10-causes-of-death

[4] B. W. Streeter and M. E. Davis, "Therapeutic Cardiac Patches for Repairing the Myocardium," in *Cell Biology and Translational Medicine, Volume 5*, vol. 1144, K. Turksen, Ed., in Advances in Experimental Medicine and Biology, vol. 1144. , Cham: Springer International Publishing, 2018, pp. 1–24. doi: 10.1007/5584_2018_309.

[5] S. McMahan, A. Taylor, K. M. Copeland, Z. Pan, J. Liao, and Y. Hong, "Current advances in biodegradable synthetic polymer based cardiac patches," *Journal of Biomedical Materials Research Part A*, vol. 108, no. 4, pp. 972–983, 2020, doi: 10.1002/jbm.a.36874.

[6] D. K. C. Cooper and E. Cozzi, "Clinical Pig Heart Xenotransplantation—Where Do We Go From Here?," *Transpl Int*, vol. 37, p. 12592, Feb. 2024, doi: 10.3389/ti.2024.12592.

[7] J. Zhang, W. Zhu, M. Radisic, and G. Vunjak-Novakovic, "Can We Engineer a Human Cardiac Patch for Therapy?," *Circ Res*, vol. 123, no. 2, pp. 244–265, Jul. 2018, doi: 10.1161/CIRCRESAHA.118.311213.

[8] M. Kitsara, O. Agbulut, D. Kontziampasis, Y. Chen, and P. Menasché, "Fibers for hearts: A critical review on electrospinning for cardiac tissue engineering," *Acta Biomaterialia*, vol. 48, pp. 20–40, Jan. 2017, doi: 10.1016/j.actbio.2016.11.014.

[9] A. M. E. Abdalla, Y. Miao, A. I. M. Ahmed, N. Meng, and C. Ouyang, "CAR-T cell therapeutic avenue for fighting cardiac fibrosis: Roadblocks and perspectives," *Cell Biochemistry and Function*, vol. 42, no. 2, p. e3955, 2024, doi: 10.1002/cbf.3955.

[10] R. J. Vagnozzi, A. K. Z. Johansen, and J. D. Molkentin, "CARdiac Immunotherapy: T Cells Engineered to Treat the Fibrotic Heart," *Molecular Therapy*, vol. 27, no. 11, pp. 1869–1871, Nov. 2019, doi: 10.1016/j.ymthe.2019.09.021.

[11] A. K. Capulli, L. A. MacQueen, S. P. Sheehy, and K. K. Parker, "Fibrous scaffolds for building hearts and heart parts," *Advanced Drug Delivery Reviews*, vol. 96, pp. 83–102, Jan. 2016, doi: 10.1016/j.addr.2015.11.020.

[12] Britannica, The Editors of Encyclopaedia, "Cardiac muscle | Definition, Function, & Structure | Britannica," Encyclopedia Britannica. Accessed: Aug. 01, 2024. [Online]. Available: https://www.britannica.com/science/cardiac-muscle

[13] M. Kharaziha *et al.*, "PGS:Gelatin nanofibrous scaffolds with tunable mechanical and structural properties for engineering cardiac tissues," *Biomaterials*, vol. 34, no. 27, pp. 6355–6366, Sep. 2013, doi: 10.1016/j.biomaterials.2013.04.045.

[14] E. Boland, F. Quondamatteo, and T. Van Agtmael, "The role of basement membranes in cardiac biology and disease," *Bioscience Reports*, vol. 41, no. 8, p. BSR20204185, Aug. 2021, doi: 10.1042/BSR20204185.

[15] N. J. Kaiser and K. L. K. Coulombe, "Physiologically inspired cardiac scaffolds for tailored in vivo function and heart regeneration," *Biomed. Mater.*, vol. 10, no. 3, p. 034003, May 2015, doi: 10.1088/1748-6041/10/3/034003.

[16] C. A. Wu, Y. Zhu, and Y. J. Woo, "Advances in 3D Bioprinting: Techniques, Applications, and Future Directions for Cardiac Tissue Engineering," *Bioengineering*, vol. 10, no. 7, Art. no. 7, Jul. 2023, doi: 10.3390/bioengineering10070842.

[17] P. Rider, Ž. P. Kačarević, S. Alkildani, S. Retnasingh, and M. Barbeck, "Bioprinting of tissue engineering scaffolds," *J Tissue Eng*, vol. 9, p. 2041731418802090, Jan. 2018, doi: 10.1177/2041731418802090.

[18] W. S. Toh and X. J. Loh, "Advances in hydrogel delivery systems for tissue regeneration," *Materials Science and Engineering: C*, vol. 45, pp. 690–697, Dec. 2014, doi: 10.1016/j.msec.2014.04.026.

[19] L. R. Feksa, E. A. Troian, C. D. Muller, F. Viegas, A. B. Machado, and V. C. Rech, "Chapter 11 - Hydrogels for biomedical applications," in *Nanostructures for the Engineering of Cells, Tissues and Organs*, A. M. Grumezescu, Ed., William Andrew Publishing, 2018, pp. 403–438. doi: 10.1016/B978-0-12-813665-2.00011-9.

[20] B. Peña *et al.*, "Injectable Hydrogels for Cardiac Tissue Engineering," *Macromolecular Bioscience*, vol. 18, no. 6, p. 1800079, 2018, doi: 10.1002/mabi.201800079.

[21] A. Mousavi, S. Mashayekhan, N. Baheiraei, and A. Pourjavadi, "Biohybrid oxidized alginate/myocardial extracellular matrix injectable hydrogels with improved electromechanical properties for cardiac tissue engineering," *International Journal of Biological Macromolecules*, vol. 180, pp. 692–708, Jun. 2021, doi: 10.1016/j.ijbiomac.2021.03.097.

[22] M. A. Abdul Sisak, F. Louis, and M. Matsusaki, "In vitro fabrication and application of engineered vascular hydrogels," *Polym J*, vol. 52, no. 8, pp. 871–881, Aug. 2020, doi: 10.1038/s41428-020-0331-z.

[23] M. Boffito, S. Sartori, and G. Ciardelli, "Polymeric scaffolds for cardiac tissue engineering: requirements and fabrication technologies," *Polymer International*, vol. 63, no. 1, pp. 2–11, 2014, doi: 10.1002/pi.4608.

[24] Q.-Z. Chen *et al.*, "Characterisation of a soft elastomer poly(glycerol sebacate) designed to match the mechanical properties of myocardial tissue," *Biomaterials*, vol. 29, no. 1, pp. 47–57, Jan. 2008, doi: 10.1016/j.biomaterials.2007.09.010.

[25] K. E. Kadler, C. Baldock, J. Bella, and R. P. Boot-Handford, "Collagens at a glance," *Journal of Cell Science*, vol. 120, no. 12, pp. 1955–1958, Jun. 2007, doi: 10.1242/jcs.03453.

[26] J. G. Stinstra, B. Hopenfeld, and R. S. MacLeod, “On the Passive Cardiac Conductivity,” *Ann Biomed Eng*, vol. 33, no. 12, pp. 1743–1751, Dec. 2005, doi: 10.1007/s10439-005-7257-7.

[27] E. Rezvani Ghomi *et al.*, “Advances in electrospinning of aligned nanofiber scaffolds used for wound dressings,” *Current Opinion in Biomedical Engineering*, vol. 22, p. 100393, Jun. 2022, doi: 10.1016/j.cobme.2022.100393.

[28] N. G. Rim, C. S. Shin, and H. Shin, “Current approaches to electrospun nanofibers for tissue engineering,” *Biomed. Mater.*, vol. 8, no. 1, p. 014102, Jan. 2013, doi: 10.1088/1748-6041/8/1/014102.

[29] B. Robb and B. Lennox, “3 - The electrospinning process, conditions and control,” in *Electrospinning for Tissue Regeneration*, L. A. Bosworth and S. Downes, Eds., in Woodhead Publishing Series in Biomaterials. , Woodhead Publishing, 2011, pp. 51–66. doi: 10.1533/9780857092915.1.51.

[30] S. Cesur *et al.*, “Production and characterization of elastomeric cardiac tissue-like patches for Myocardial Tissue Engineering,” *Polymer Testing*, vol. 90, p. 106613, Oct. 2020, doi: 10.1016/j.polymertesting.2020.106613.

[31] O. Gil-Castell, I. Ontoria-Oviedo, J. D. Badia, E. Amaro-Prellezo, P. Sepúlveda, and A. Ribes-Greus, “Conductive polycaprolactone/gelatin/polyaniline nanofibres as functional scaffolds for cardiac tissue regeneration,” *Reactive and Functional Polymers*, vol. 170, p. 105064, Jan. 2022, doi: 10.1016/j.reactfunctpolym.2021.105064.

[32] Y. Liu, S. Wang, and R. Zhang, “Composite poly(lactic acid)/chitosan nanofibrous scaffolds for cardiac tissue engineering,” *International Journal of Biological Macromolecules*, vol. 103, pp. 1130–1137, Oct. 2017, doi: 10.1016/j.ijbiomac.2017.05.101.

[33] G. Zhao *et al.*, “Anisotropic conductive reduced graphene oxide/silk matrices promote post-infarction myocardial function by restoring electrical integrity,” *Acta Biomaterialia*, vol. 139, pp. 190–203, Feb. 2022, doi: 10.1016/j.actbio.2021.03.073.

[34] N. Shokraei, S. Asadpour, S. Shokraei, M. Nasrollahzadeh Sabet, R. Faridi-Majidi, and H. Ghanbari, “Development of electrically conductive hybrid nanofibers based on CNT-polyurethane nanocomposite for cardiac tissue engineering,” *Microscopy Research and Technique*, vol. 82, no. 8, pp. 1316–1325, 2019, doi: 10.1002/jemt.23282.

[35] C. Mancino *et al.*, “Electrospun electroconductive constructs of aligned fibers for cardiac tissue engineering,” *Nanomedicine: Nanotechnology, Biology and Medicine*, vol. 44, p. 102567, Aug. 2022, doi: 10.1016/j.nano.2022.102567.

[36] M. Wanjare *et al.*, “Anisotropic microfibrous scaffolds enhance the organization and function of cardiomyocytes derived from induced pluripotent stem cells,” *Biomater. Sci.*, vol. 5, no. 8, pp. 1567–1578, Jul. 2017, doi: 10.1039/C7BM00323D.

[37] H. Esmaeili *et al.*, “Electroconductive biomaterials for cardiac tissue engineering,” *Acta Biomaterialia*, vol. 139, pp. 118–140, Feb. 2022, doi: 10.1016/j.actbio.2021.08.031.

[38] Y. Li *et al.*, “Conductive biomaterials for cardiac repair: A review,” *Acta Biomaterialia*, vol. 139, pp. 157–178, Feb. 2022, doi: 10.1016/j.actbio.2021.04.018.

[39] A. Fakhrali *et al.*, “Biocompatible graphene-embedded PCL/PGS-based nanofibrous scaffolds: A potential application for cardiac tissue regeneration,” *Journal of Applied Polymer Science*, vol. 138, no. 40, p. 51177, 2021, doi: 10.1002/app.51177.

[40] Y. Tan *et al.*, “Engineering a conduction-consistent cardiac patch with rGO/PLCL electrospun nanofibrous membranes and human iPSC-derived cardiomyocytes,” *Frontiers in Bioengineering and Biotechnology*, vol. 11, 2023, Accessed: Jan. 08, 2024. [Online]. Available: https://www.frontiersin.org/articles/10.3389/fbioe.2023.1094397

[41] M. Shevach, B. M. Maoz, R. Feiner, A. Shapira, and T. Dvir, “Nanoengineering gold particle composite fibers for cardiac tissue engineering,” *J. Mater. Chem. B*, vol. 1, no. 39, pp. 5210–5217, Sep. 2013, doi: 10.1039/C3TB20584C.

[42] K. Roshanbinfar, L. Vogt, F. Ruther, J. A. Roether, A. R. Boccaccini, and F. B. Engel, “Nanofibrous Composite with Tailorable Electrical and Mechanical Properties for Cardiac Tissue Engineering,” *Adv. Funct. Mater.*, vol. 30, no. 7, p. 1908612, Feb. 2020, doi: 10.1002/adfm.201908612.

[43] A. Abedi, M. Hasanzadeh, and L. Tayebi, “Conductive nanofibrous Chitosan/PEDOT:PSS tissue engineering scaffolds,” *Materials Chemistry and Physics*, vol. 237, p. 121882, Nov. 2019, doi: 10.1016/j.matchemphys.2019.121882.

[44] S. Nemati, S. Kim, Y. M. Shin, and H. Shin, “Current progress in application of polymeric nanofibers to tissue engineering,” *Nano Convergence*, vol. 6, no. 1, p. 36, Nov. 2019, doi: 10.1186/s40580-019-0209-y.

[45] L. Martocq and T. E. L. Douglas, “Amine-Rich Coatings to Potentially Promote Cell Adhesion, Proliferation and Differentiation, and Reduce Microbial Colonization: Strategies for Generation and Characterization,” *Coatings*, vol. 11, no. 8, Art. no. 8, Aug. 2021, doi: 10.3390/coatings11080983.

[46] K. S. Siow, L. Britcher, S. Kumar, and H. J. Griesser, “Plasma Methods for the Generation of Chemically Reactive Surfaces for Biomolecule Immobilization and Cell Colonization - A Review,” *Plasma Processes and Polymers*, vol. 3, no. 6–7, pp. 392–418, 2006, doi: 10.1002/ppap.200600021.

[47] H. Savoji, A. Hadjizadeh, M. Maire, A. Ajji, M. R. Wertheimer, and S. Lerouge, “Electrospun Nanofiber Scaffolds and Plasma Polymerization: A Promising Combination Towards Complete, Stable Endothelial Lining for Vascular Graft,” *Macromol. Biosci.*, vol. 14, no. 8, pp. 1084–1095, Aug. 2014, doi: 10.1002/mabi.201300545.

[48] A. Jafari *et al.*, “Combination of 3D Printing, Plasma Polymerization, and Bioactive Coatings Towards Fabrication of Eggshell Biowaste/Polycaprolactone Composite Scaffolds for Bone Regeneration,” *Adv Compos Hybrid Mater*, vol. 7, no. 4, p. 131, Aug. 2024, doi: 10.1007/s42114-024-00932-4.

[49] J.-C. Ruiz, A. St-Georges-Robillard, C. Thérésy, S. Lerouge, and M. R. Wertheimer, “Fabrication and Characterisation of Amine-Rich Organic Thin Films: Focus on Stability,” *Plasma Processes and Polymers*, vol. 7, no. 9–10, pp. 737–753, 2010, doi: 10.1002/ppap.201000042.

[50] J.-C. Ruiz, P.-L. Girard-Lauriault, and F. Truica-Marasescu, “Plasma and vacuum-ultraviolet (VUV) photo-polymerisation of N- and O-rich thin films,” *Radiation Physics and*

Chemistry - RADIAT PHYS CHEM, vol. 79, pp. 310–314, Mar. 2010, doi: 10.1016/j.radphyschem.2009.08.009.

[51] P.-L. Girard-Lauriault *et al.*, "Adhesion of Human U937 Monocytes to Nitrogen-Rich Organic Thin Films: Novel Insights into the Mechanism of Cellular Adhesion," *Macromolecular Bioscience*, vol. 9, no. 9, pp. 911–921, 2009, doi: 10.1002/mabi.200800359.

[52] X. Jin, J. Dong, X. Guo, M. Ding, R. Bao, and Y. Luo, "Current advances in polyurethane biodegradation," *Polymer International*, vol. 71, no. 12, pp. 1384–1392, 2022, doi: 10.1002/pi.6360.

[53] K. Tadyszak, J. K. Wychowaniec, and J. Litowczenko, "Biomedical Applications of Graphene-Based Structures," *Nanomaterials*, vol. 8, no. 11, Art. no. 11, Nov. 2018, doi: 10.3390/nano8110944.

[54] F. Truica-Marasescu and M. R. Wertheimer, "Nitrogen-Rich Plasma-Polymer Films for Biomedical Applications," *Plasma Processes & Polymers*, vol. 5, no. 1, pp. 44–57, Jan. 2008, doi: 10.1002/ppap.200700077.

[55] S. Fleischer *et al.*, "Spring-like fibers for cardiac tissue engineering," *Biomaterials*, vol. 34, no. 34, pp. 8599–8606, Nov. 2013, doi: 10.1016/j.biomaterials.2013.07.054.

[56] S. Jang *et al.*, "Biomechanical and Hemodynamic Measures of Right Ventricular Diastolic Function: Translating Tissue Biomechanics to Clinical Relevance," *J Am Heart Assoc*, vol. 6, no. 9, p. e006084, Sep. 2017, doi: 10.1161/JAHA.117.006084.

[57] K. Kulasinski, "Effects of water adsorption in hydrophilic polymers," 2016, pp. 217–223.

[58] M. Ghasemi, S. Liang, Q. M. Luu, and I. Kempson, "The MTT Assay: A Method for Error Minimization and Interpretation in Measuring Cytotoxicity and Estimating Cell Viability," in *Cell Viability Assays: Methods and Protocols*, O. Friedrich and D. F. Gilbert, Eds., New York, NY: Springer US, 2023, pp. 15–33. doi: 10.1007/978-1-0716-3052-5_2.

[59] A. Najafi Tireh Shabankareh, P. Samadi Pakchin, M. Hasany, and H. Ghanbari, "Development of a new electroconductive nanofibrous cardiac patch based on polyurethane-reduced graphene oxide nanocomposite scaffolds," *Materials Chemistry and Physics*, vol. 305, p. 127961, Sep. 2023, doi: 10.1016/j.matchemphys.2023.127961.

[60] E. Vatankhah, M. P. Prabhakaran, D. Semnani, S. Razavi, M. Morshed, and S. Ramakrishna, "Electrospun tecophilic/gelatin nanofibers with potential for small diameter blood vessel tissue engineering," *Biopolymers*, vol. 101, no. 12, pp. 1165–1180, 2014, doi: 10.1002/bip.22524.

[61] A. Gostev *et al.*, "In Vivo Stability of Polyurethane-Based Electrospun Vascular Grafts in Terms of Chemistry and Mechanics," *Polymers*, vol. 12, no. 4, p. 845, Apr. 2020, doi: 10.3390/polym12040845.

[62] A. G. Guex *et al.*, "Fine-tuning of substrate architecture and surface chemistry promotes muscle tissue development," *Acta Biomaterialia*, vol. 8, no. 4, pp. 1481–1489, Apr. 2012, doi: 10.1016/j.actbio.2011.12.033.

APPENDIX A FIBER DIAMETER DISTRIBUTION HISTOGRAMS

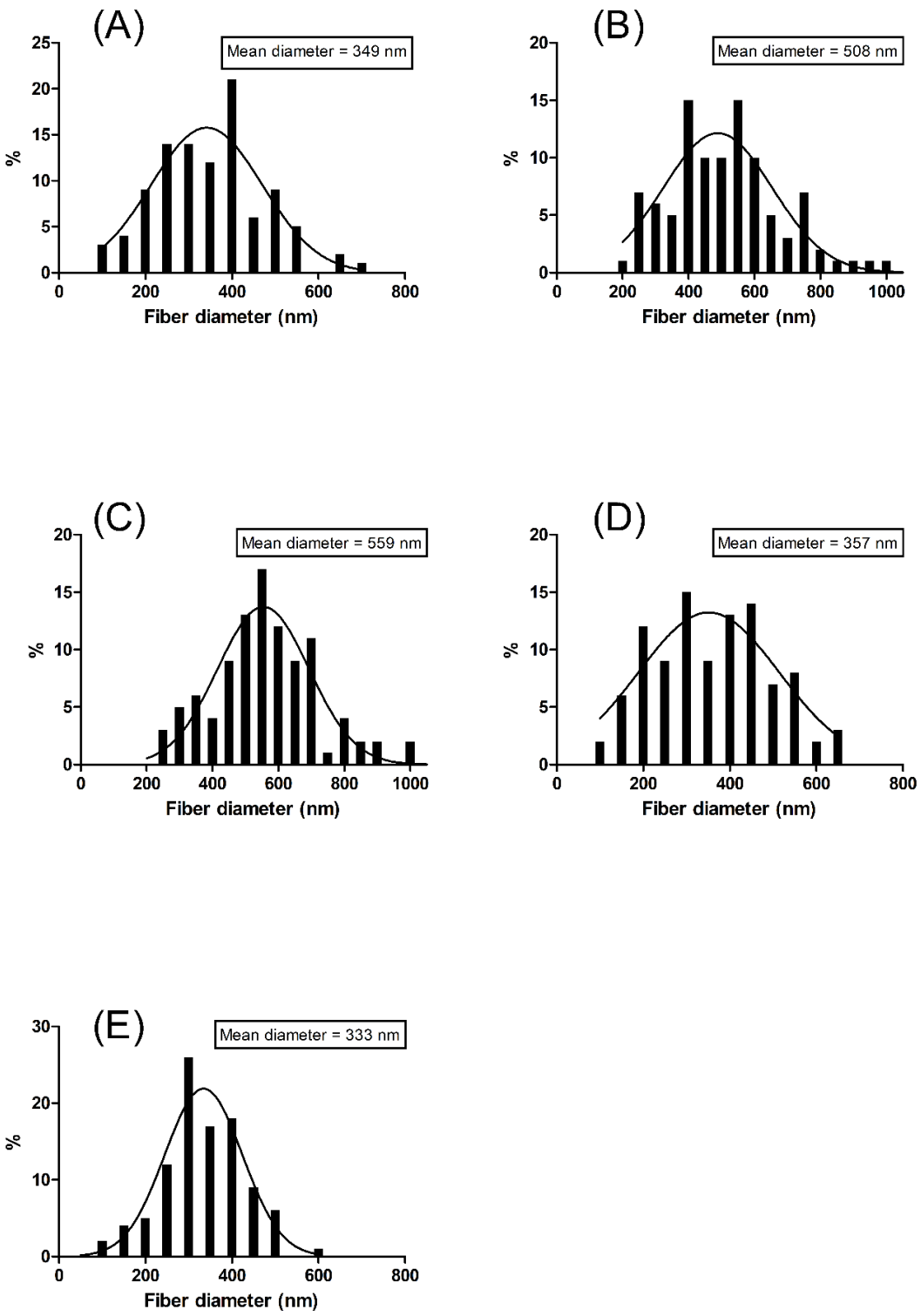

Figure A.1 : Fiber diameter distribution histograms of electrospun mats. (A) PU R. (B) PU A. (C) PU R-A. (D) PU rGO0.5. (E) PU rGO1. (n=100)

APPENDIX B FIBER ORIENTATION DISTRIBUTION HISTOGRAMS

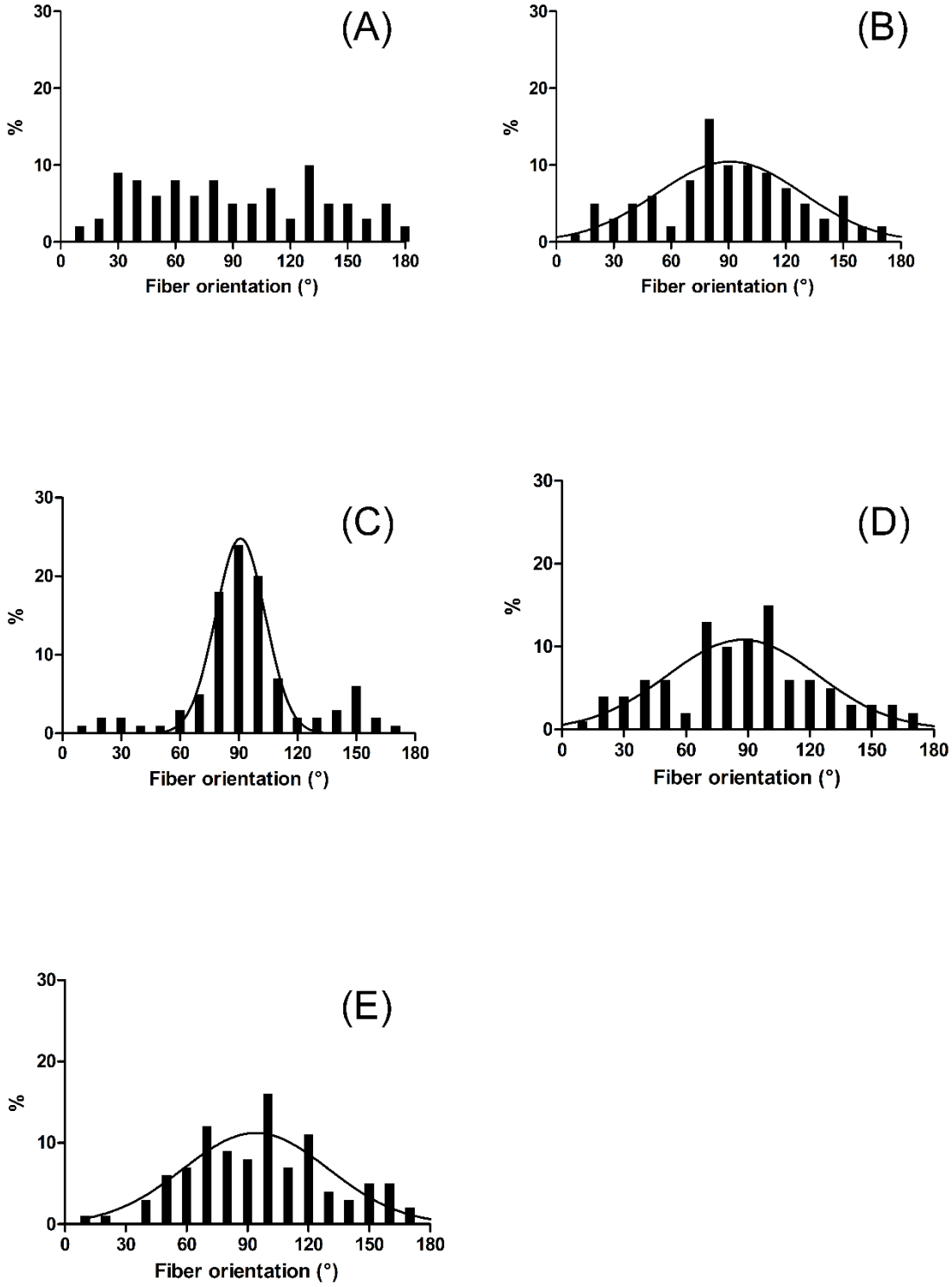

Figure B.1 : Fiber orientation distribution histograms of electrospun mats. (A) PU R. (B) PU A. (C) PU R-A. (D) PU rGO0.5. (E) PU rGO1. (n=100)

APPENDIX C INDIRECT LIVE/DEAD ASSAY QUANTIFICATION

Table C.1 : Cell counts and viability from Live/Dead images of indirect cytotoxicity assessment

	Viable cells (green)	**Dead cells (red)**	**Viability**
TCP	143	8	94.7%
PU	868	7	99.2%
PU rGO0.5	401	5	98.8%
PU rGO0.5 LPPE:N	373	8	97.9%
PU rGO1	190	3	98.4%
PU rGO1 LPPE:N	254	3	98.8%